High-Contrast Origins Science for NGST

Pre-Phase A Science Instrumentation Concept Study Report for the
Next Generation Space Telescope (NGST)
In response to NRA 98-GSFC-1

INVESTIGATORS
John Trauger[1] PI, Karl Stapelfeldt[1], Raghvendra Sahai[1],
Dana Backman[2], Charles Beichman[4], George Djorgovski[3], Mark Ealey[6],
Eric Gaidos[1], Carl Grillmair[4], Yekta Gürsel[1], Shrinivas Kulkarni[3],
Richard Lyon[5]; Steven Macenka[1]; Christopher Martin[3], Michael Ressler[1],
Michael Shao[1], Michael Werner[1]

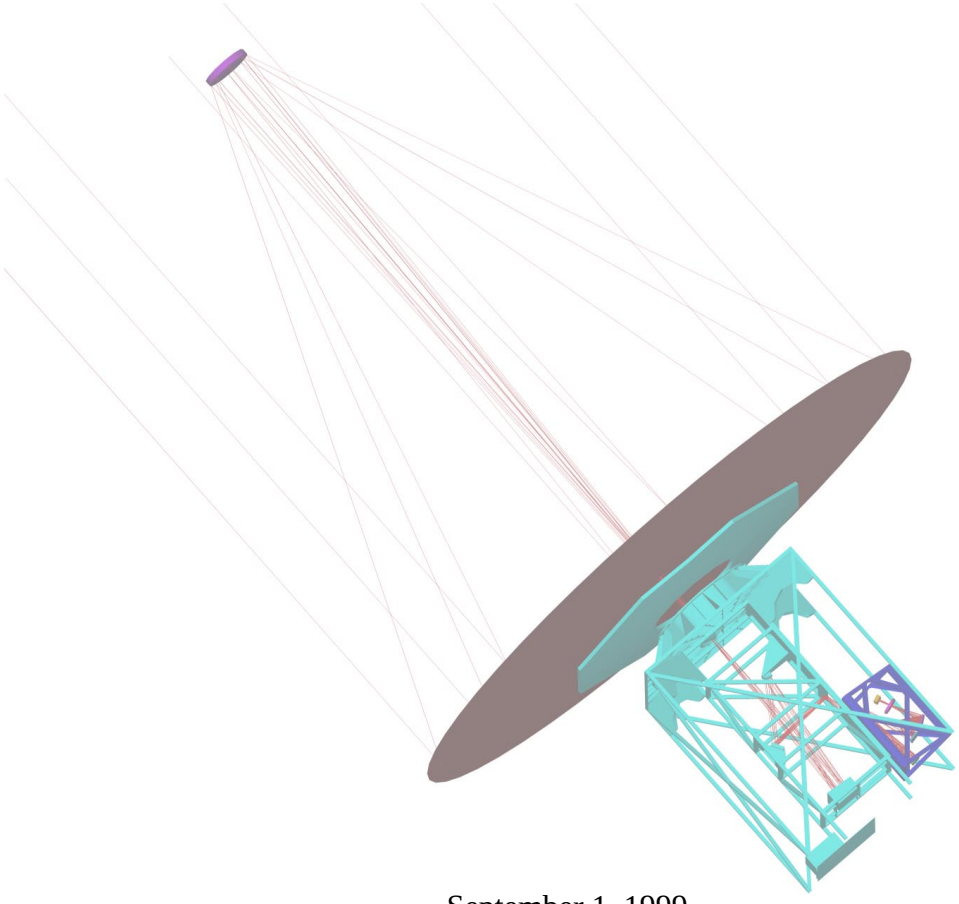

September 1, 1999

Affiliations: [1]Jet Propulsion Laboratory; [2]Franklin & Marshall College; [3]California Institute of Technology; [4]JPL/IPAC; [5]Goddard Space Flight Center; [6]Xinetics, Inc.

TABLE OF CONTENTS

1. SCIENCE 1-1

1.1 Executive Summary 1-1

1.2 Science Capability 1-1

1.2.1 Extra-Solar Giant Planets & Brown Dwarf Companions 1-2

1.2.2 Young Stellar Objects 1-6

1.2.3 Debris Disks and Structures 1-8

1.2.4 Near-Environment of AGB and Post-AGB Stars 1-9

1.2.5 QSO Origins and Host Galaxies 1-11

1.3 Historical Setting for CCM 1-12

1.3.1 Hubble Space Telescope 1-12

1.3.2 Results from SIRTF and SOFIA 1-13

1.3.3 Astrometric and Radial Velocity Planet Searches 1-13

1.3.4 Large Ground-based and Balloon Telescopes with Adaptive Optics 1-14

1.3.5 Space-based Nulling Interferometry 1-14

2. ENGINEERING 2-1

2.1 Design Concept 2-1

2.1.1 ISIM Environment 2-1

2.1.2 Optomechanical Design 2-2

2.1.3 CCM Optical Design 2-2

2.1.4 Structure Volume and Mass 2-3

2.1.5 Passive Athermalization 2-4

2.1.6 Mechanisms 2-5

2.1.6.1 Cassini Heritage Filter Wheel 2-5

2.1.6.2 WFPC2 Heritage Active Mirror 2-6

2.1.6.3 Lyot x/y Translation Stage 2-7

2.1.7 NIR Detector Characteristics 2-7

2.1.8 Image Stabilization and Pointing 2-7

2.1.9 Coronagraph Design 2-8

2.1.10 NGST/CCM Imaging Simulations 2-8

2.2 Technology Readiness 2-10

2.3 Development Schedule and I&T Plan 2-12

Table of Contents (cont'd)

3. COST ESTIMATE 3-1

3.1 Cost Summary 3-1

3.2 WBS and Cost Breakdown 3-2

4. REFERENCES 4-1

1. SCIENCE

1.1 Executive Summary

This report presents the results of a coronagraphic camera concept study for the NGST ISIM. We find that a coronagraph camera module (CCM) will enable unique, high-contrast imaging astronomy that enhances the core NGST science capabilities in the near-infrared. This study has identified a number of exciting science opportunities for NGST, and based on high-fidelity modeling it has evaluated the engineering prerequisites needed to take advantage of these opportunities.

With its large aperture, from the vantage of space, the NGST provides an unprecedented opportunity for the high resolution and extremely high contrast imaging needed to observe a representative sample of planets, substellar companions, and reflection nebulae associated with embryonic and evolved stellar systems in our galactic neighborhood. The discovery space for a NGST coronagraph extends from the complex environments of the nearest stars to the engines that power AGN in distant galaxies. CCM provides coverage from 1 to 5 μm with a 52×52 arcsecond field of view. A filter wheel provides a selection of optical filters (R ~ 5–10) and grisms (R ~ 100) as required for the science programs. We have considered five broad scientific objectives that are prominent components of NASA's Origins program.

The performance of a NGST coronagraph depends intimately on the system characteristics of the NGST optical telescope assembly (OTA) and the shared optical elements of the ISIM. In particular, the surface finish and alignment of the lightweight segmented primary mirror, the detailed characteristics of the selected wavefront correcting technology, the placement and performance of the fast steering mirror, and overall stability of the optical system on short timescales play prominent roles. A detailed study of coronagraph designs and performance for a number of NGST system architectures has been considered. A robust science program is made possible with a coronagraph in a variety of NGST system architectures. We have considered an instrument concept that provides additional internal wavefront correction, based on recent deformable mirror technology developments. However, based on reasonable projections of the NGST optical performance, the additional complexity of internal wavefront correction is not required to enable major additions to the NGST science program. With careful attention to key optical specifications and the wavefront correction technology that NGST selects, the reach of NGST's science observing programs can be enhanced in a cost-effective manner.

The CCM is feasible without the development of new high-risk technologies. Our engineering assessment indicates that only three mechanisms are needed for CCM. The most important of these is a filter selector mechanism that draws on Cassini, WFPC2, and cryogenic instrumentation heritage. An internal image dither mechanism is included, again adapted from an existing flight hardware design. A positioning mechanism is specified for fine alignment of the CCM optical axis. These mechanisms are compatible with NGST's unusual thermal requirements. The cost of CCM is moderate, the instrument footprint is small in terms of volume, mass, power, and required field of view, and a number of descope options are available.

In addition to the unique, pioneering science that a coronagraph adds, it can also assist with wavefront management for the entire suite of NGST instruments by providing high contrast analysis of the PSF wings as feedback for the optimal adjustment of NGST's deformable mirror.

1.2 Science Capability

The circumstellar environment is a key arena for scientific progress in NASA's Origins program. To directly study planetary systems in our galactic neighborhood, the disks from which they form, and the detailed stages of their demise, we must reach into the glare of the central star and uncover what has heretofore been hidden. This study has considered the scientific potential and engineering requirements for ground-breaking circumstellar research with NGST in four key areas: (1) the structures surrounding young stellar objects, including protoplanetary disks, gaseous jets, and very young planets still radiating their accretion energy; (2) the nature of mature planets and brown dwarf companions in the solar neighborhood; (3) the properties of tenuous exozodiacal debris disks in more evolved planetary systems, and (4) the processes by which evolved stars expel their harvest of heavy elements into the galactic medium, providing raw material for the next

generation of stars and planets. Beyond our galactic neighborhood, this instrument concept also offers important discovery potential in bright quasar environments.

1.2.1 Extra-Solar Giant Planets & Brown Dwarf Companions

One of the central scientific objectives for NGST/CCM is the direct detection of jovian planets orbiting stars in the solar neighborhood. The challenge of direct exoplanet detection has been well-documented in various NASA studies, most recently the 1996 ExNPS road map, and is now a key goal of NASA's Origins program. Direct imaging will provide brightness and color information that cannot be obtained from indirect astrometric and radial velocity measurements. Exoplanet photometry is fundamental data needed to characterize the luminosity, temperature, and atmospheric structure of these objects, and to place them in context with the planets of our solar system. The exciting discoveries of planetary companions from radial velocity surveys of solar-type stars (Mayor & Queloz 1995, Marcy & Butler 1998, Cochran *et al.* 1997) has proved for the first time that other planetary systems exist, and that they can be very different from our own.

Similarly, the discovery of the cool brown dwarf companion GL229B (Nakajima *et al.* 1995) has led to a major resurgence of interest in the faint end of the stellar luminosity function. Brown dwarfs (BDs) are gaseous objects intermediate in mass between Jovian planets and stars; with masses $< \sim 0.08\ M_{\odot}$, they never obtain the core pressures and temperatures required for hydrogen fusion.

It is generally believed that BDs (like low-mass stars) form through the collapse of dense molecular cloud cores, and that planets form in circumstellar disks through coagulation of planetesimals. However, we currently do not know the range of companion masses that can be produced by these two formation mechanisms, or if those two ranges overlap. A low-mass cutoff is expected for brown dwarfs, associated with the fragmentation process which produces dense cloud cores. However, substantial mass evolution may occur due to the dynamic environment in which they are immersed at early ages. An upper limit to the mass of planets may be determined by the limited supply of material available in proto-planetary disks.

The large eccentricities and small separations found for many of the extrasolar giant planets (EGPs) has spurred new debate on the formation and orbital stability of planetary systems (e.g. inward orbital migration of EGPs due to viscous losses in the residual protoplanetary disk), and the possible similarities and differences in the formation processes of EGPs and BDs. Planet formation may well have proceeded very differently around stars of different mass than the Sun, or under different initial conditions. Unfortunately, our understanding of these issues is extremely poor because the number of detected BD/EGP companions remains quite small. A decade of extensive observational effort has been rewarded with today's capability to detect and study *isolated* brown dwarfs in their own intrinsic thermal emission. However, the detected objects are either relatively young (age < 1 Gyr) or massive ($\sim$ few $\times$ 10 M_J). For fainter (older or less massive) objects, the detection statistics are dismal: only one cold ($T_{eff} < 1000K$) "methane" brown dwarf *companion* has been found so far. No BD/EGP companions have been directly detected in the 0.3–30 AU range of separations corresponding to planets in our solar system. The detection and characterization of these substellar companions represents a new astrophysical frontier that should produce insights into several key issues such as binary star formation, accretion processes in protoplanetary disks, and the nature of dark matter.

Significant advances will require the ability to obtain a reasonably complete census of BDs/EGPs, both in isolation and in orbit around stars (e.g. covering a range of masses, primary star spectral type, and orbital separations). As a follow-up to such a survey, spectra of a range of different BDs/EGPs are highly desirable to constrain their physical properties, including temperature and luminosity as a function of age, their gravity, and the presence of molecules in their atmospheres. Detection and characterization of EGPs is an important first step that NGST can provide in the study of other planetary systems.

Full-sky ground-based infrared surveys such as DENIS and 2MASS are steadily building up the detection statistics for isolated brown dwarfs (Burgasser *et al.* 1999, Strauss *et al.* 1999). Large telescopes and interferometers with adaptive optics should soon make initial direct detections of BD companions of

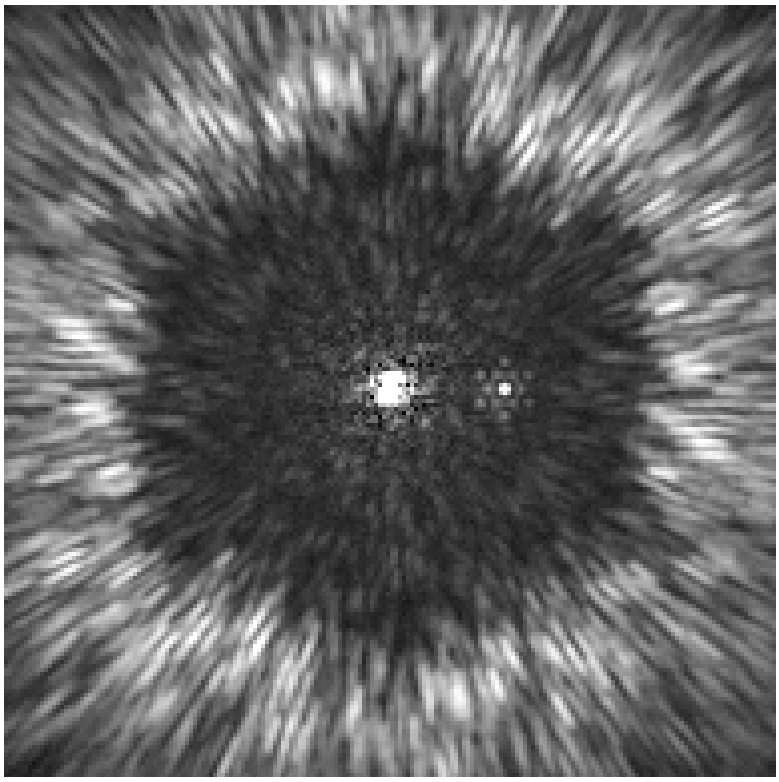

Figure 1-1 *Simulated NGST/ CCM image of Lalande 21185 (a main-sequence M2 dwarf located at 2.5 pc) with an assumed jovian planet at 5AU distance, taken in a single M band exposure of 0.5 hours. A very large brightness enhancement beyond blackbody is predicted for methane-blanketed giant planets and brown dwarfs at M (Burrows* et al. *1997). The detectibility of younger and/or more massive companions is more favorable still than the case for 5GY jupiters.*

nearby stars. However, such observations will be limited to the bright end (high mass/low age) of the BD luminosity function, and to wide binary separations for the detected companions. Indirect search techniques such as radial velocity or astrometric measurements of the primary star (soon feasible with ground- and space- based interferometers) provide important complementary information (the companion's minimum mass, and its orbital period), but also suffer selection effects toward higher masses and short orbital periods. The indirect techniques provide no photons from the BDs/EGPs, leaving us to speculate as to the luminosity and spectral character of these new worlds.

A major opportunity for observational progress is available to NGST if it is equipped with a suitable coronagraphic camera. NGST's unsurpassed sensitivity at near- and mid-infrared wavelengths, combined with its high spatial resolution and stable PSF, will facilitate pioneering work that includes the detection and characterization of substellar companions of nearby stars. These capabilities are not contemplated for any other observatory that will be available before the end of the next decade. SIRTF will have the sensitivity to detect isolated BDs, but lacks the spatial resolution to distinguish them as companions on solar-system scales. Large ground-based telescopes with adaptive optics will offer the angular resolution needed to resolve BD companions from their parent stars, but their high backgrounds and contrast limitations will restrict their contributions to the most luminous objects at the largest separations. With the proper instrumentation, NGST can bridge this gap by facilitating the direct detection of substellar companions of nearby stars, including objects whose masses and ages are comparable to our own Jupiter and Saturn, and whose orbital positions fall in the range of 5–10 AU. Direct detection has the added advantage that it is no more difficult to detect complex systems with multiple planets than a single planetary companion. It provides the means to further investigate many planetary systems discovered in groundbased radial velocity searches, including the recent discovery of three EPGs around υ Andromedae (Butler *et al.* 1999) and others that will inevitably be discovered in the next several years.

We have used coronagraphic instrument performance models to compute detailed estimates of the NGST optical performance that

include with a measure of optimism the optical characteristics and operational procedures presently anticipated for NGST. A seven-hexagon deployed primary mirror is assumed, following the system architecture study of TRW. Provision is made for wavefront correction on the primary mirror, with up to 394 actuators working on each hexagonal segment according to the Arizona mirror design concept (Angel and Burge 1999). The optical alignment procedures of D. Redding (private communication) are implemented as follows. First, the seven individual mirror segments are assigned surface figure errors with power spectral densities (PSDs) comparable to the HST primary mirror (see Section 2.1.10). Next, the seven randomly misaligned mirror segments are brought into alignment by wavefront retrieval of a star image. Finally, the mirror actuators are used to further refine the optical wavefront through phase retrieval of a star image. This alignment procedure terminates when the diffraction limit is achieved at 2 μm wavelength. We emphasize that *no further wavefront corrections* are assumed for the CCM science described in this report.

The effects of scattering and diffraction in the instrument are combined with backgrounds from solar system zodiacal emission and emission from the telescope primary to estimate the background level against which a planet must be detected. Shot noise on this background and detector noise are combined together to estimate integration times for planet detection at S/N = 10. This is a somewhat conservative detection criterion, since planets will always appear as point-like images whereas residual speckles take on a spectrally dispersed and streaked appearance in broad-band images. Additional image processing with spatial filtering should provide better sensitivity, but is not assumed in our feasibility criterion. Exposure times are calculated for actual Gliese catalog objects, using their apparent magnitudes and distances (Gliese and Jahreiss, 1979).

Our investigation of the expected 1–5 μm emission from EGPs/BDs and the corresponding sensitivity of CCM, taking into account the strongly wavelength dependent backgrounds, shows that 5 μm is an especially attractive wavelength for the study of Jovian planets and brown dwarfs. At this wavelength, atmospheres with T_{eff} < 1200K are significantly cleared of molecular opacity, allowing thermal emission from warmer, deeper levels of the objects to escape directly to space. It has long been known that Jupiter's disk shows broad "hot spots" in 5 μm images (Ortiz *et al.* 1998). The spectrum of GL229B also shows a prominent flux enhancement at 5 μm (Oppenheimer *et al.* 1998). Theoretical spectra from model brown dwarf atmospheres consistently show the same bright emission near 5 μm, and indicate that these objects can be *many orders of magnitude* brighter than an equivalent blackbody radiator at the planet's effective temperature (Burrows *et al.* 1997; Allard *et al.* 1996). For example, the 5 μm contrast between a Jupiter-like companion and an M star primary (such as Lalande 21185) is just 6×10^6. The superthermal emission of EGPs and BDs at 5 μm offers a distinct opportunity for planet detection that NGST should exploit.

We describe below a detailed observational program with CCM of studying jovian planet and brown dwarf companions, in light of the overriding importance of this science.

1. Search for Planets

CCM can be used to make a nearly complete search for giant planet companions in a sample of nearby single stars (d < 10 pc), aimed at detecting EGPs at least as bright as Jupiter (i.e. mass = 0.001 $M_\odot$, age = 4.5 Gyr, absolute M magnitude 23) at separations of 5 AU. Using a 10% bandwidth M filter, the survey will be able to detect Jupiters around *all* single stars within 8 pc in integration times of 3 hours or less, and around a significant fraction of others stars at greater distances. Detection of more luminous (more massive, or younger) or more widely separated companions will be correspondingly easier, and can be accomplished for progressively more distant systems from the Sun. A total of 90 targets are available within 8 pc. With integration times of < 3 hr/object, the search offers the potential to detect planets with Saturn's brightness and orbital radius in 10% of the systems within 8 pc. "Target-of-opportunity" observations can be made towards stars which indicate the presence of multiple well-separated EGP companions, as for example, in υ Andromedae (Butler *et al.* 1999).

2. SNAPSHOT Search for Extra-Solar Giant Planets/ Brown Dwarfs

CCM can be used to make a nearly complete search for brown dwarf companions in a sample of nearby single stars (d < 20 pc) in the M band, aimed at detecting BDs/EGPs

brighter than an absolute M magnitude of 19. Since the brightnesses of BDs/EGPs depend on both their masses and their ages, each observed magnitude defines a curve in the mass-age plane. For reference, either a young 1 M_J object at ~ 1 Gyr or a more massive 5 M_J object at ~ 5 Gyr would have an absolute M magnitude of 19. Using relatively short integration times (< 0.5 hr/object) (e.g. a SNAPSHOT observing mode reminiscent of HST), NGST can expect to obtain a nearly complete census of BD/EGP companions among a sample of about 500 stars.

3. Characterization of Planets and Brown Dwarfs

For the brightest objects uncovered in the two surveys above, CCM can be used to carry out spectroscopic/spectrophotometric observations from λ = 1–5 μm. R = 100 grism spectra using the coronagraph's spectral mode can be obtained for the brightest brown dwarfs. Filter photometry can be carried out for the brightest EGP companions, which will be significantly fainter than the BDs. The power of such observations for developing a detailed understanding of BDs has been demonstrated by recent observational and theoretical results on GL229B, where modeling of its strong methane (CH_4) and water (H_2O) absorption bands between 1–4 μm have provided constraints on the temperature, composition, mass, and age of the brown dwarf though comparison with a grid of atmosphere models coupled to an evolution/cooling code (Marley *et al.* 1996, Allard *et al.* 1996). CCM/NGST will thus enable us to probe the initial mass function for star formation well below the main sequence boundary. The model fitting also shows that, like Jupiter, the atmosphere of GL 229B lacks dust, indicating that metals have "rained down" or have gathered into "dust clouds" (Tsuji *et al.* 1996). The presence of clouds in these atmospheres can modify the spectrum in the 5 μm window (and in other near-IR windows), producing a more graybody spectrum depending on the particle size. The abundant water molecule is expected to be the primary cloud-forming constituent for T_{eff} < 400K; ammonia also becomes important for T_{eff} < 150K. At T_{eff} > 400K, EGP atmospheres should be relatively clear of major cloud decks, until ~ 1000K when silicates become relevant. Whether or not clouds will play a major role below 400K is uncertain, as Jupiter shows strong 5 μm emission through its very patchy water and ammonia clouds. The proposed R = 100 spectroscopic observations would provide the critical foundation for future theoretical studies which can help resolve cloud formation issues.

We estimate that with integration times of about 10 hours per object, NGST can obtain spectra with sufficient signal-to-noise to detect the major absorption bands due to water and methane expected in the (1–5) μm region. The detection of ammonia (NH_3), phosphine (PH_3), acetylene (C_2H_2), and ethylene (C_2H_6), which are prominent in Jupiter's and Saturn's spectra, could be undertaken in EGPs with the extension of the NGST wavelength baseline to 14 μm.

The two discovery surveys will be conducted in a 10% bandwidth filter centered at 4.8 μm, similar to the standard M band. The M-band is the window of choice for the survey observations because it provides the largest signal-to-noise ratio for detection. At shorter wavelengths the planet flux is significantly lower, whereas at longer wavelengths the thermal background is significantly higher. We have verified this conclusion by computing the coronagraphic performance at different wavelengths. Each target will be observed at two epochs separated by 6 months. Multiple spacecraft roll angles will be used to help discriminate detected objects from residual speckles in the NGST diffraction pattern. True companions can be identified by observing their common proper motion with the central star over the 6 month baseline. In estimating our sensitivity, we have made the conservative assumption that the substellar companion is located 45 degrees of orbital longitude from maximum elongation. This makes the observation more difficult, but ensures that planets will be detected in more than 70% of the systems where they are present. Filters specific to the features in brown dwarf/jovian planet atmospheres will be needed for the spectral characterization of faint substellar companions; these will include a 1.6 μm "methane-free" filter and special filters adjacent to M band to measure the spectral slope of the superthermal emission.

We note here that progressively higher spectral resolution observations have the potential of setting progressively stringent constraints on the characteristics of EGPs/BDs. Observations with R ~ 200 would enable one to constrain the metallicity. However,

without additional constraints (e.g. age of primary star) such low-resolution spectroscopy is still inadequate for determining the masses and ages of the detected BDs/EGPs since large mass, older BDs/EGPs have similar 1–5 μm colors and fluxes as their smaller mass but younger counterparts (Burrows *et al.* 1997). A spectral resolution of > ~ 600 is required in order to be able to estimate the gravity (hence the mass) directly from fitting (i) the spectral slope on the edges of specific bands, and (ii) the profile of narrow alkali metal absorption lines such as the 1.25 μm potassium line. The presence of water and ammonia clouds in relatively cool objects can potentially strongly affect the characteristics of the near-infrared spectrum (Marley *et al.* 1999). Disentangling the effects of clouds, from variations in their chemical composition, mass and age is probably a difficult task at a resolution R < ~ 500.

In summary, an observational program using a coronagraphic camera like CCM on NGST can be expected to provide the first determination of the giant planet/brown dwarf luminosity function and the first spectral characterization of these objects across a broad range of effective temperatures. In conjunction with mass determinations for the companions from astrometric surveys, photometric measurements with CCM will allow the theoretical cooling curves for substellar objects to be compared with actual luminosity and temperature measurements. Finally with CCM, NGST can produce the first direct images of planets orbiting other stars. The results will not only be of fundamental scientific importance to our understanding of planetary systems and their frequency in the galaxy, but also vigorously engage the public interest in NASA's ORIGINS program.

1.2.2 Young Stellar Objects

Our planetary system is believed to have formed from a flattened cloud of gas and dust which orbited the Sun very early in its history. Detailed astrophysical information on planet-forming environments is therefore obtainable via studies of the circumstellar matter of very young stars. Infrared and millimeter wavelength spectroscopic studies indicate that 50% of young stars possess circumstellar disks with masses and sizes comparable to our formative planetary system (Beckwith *et al.* 1990). Protoplanetary disks in the nearest star-forming regions have outer radii of only a few arcseconds, and their reflected light surface brightnesses (in mag/arcsec^2) are at least 10 mag fainter than the central point source. Several of these objects have now been imaged optically by HST in special circumstances of external illumination (McCaughrean and O'Dell 1996) or edge-on orientation (Burrows *et al.* 1996; Stapelfeldt *et al.* 1998), and imaged in the near-infrared using adaptive optics in a few cases (Roddier *et al.* 1996). However, HST and adaptive optics imaging have failed to detect disks in scattered light around the majority of young stars studied thus far—even though millimeter maps and infrared photometry clearly indicate that resolvable disks are present in the systems (McCaughrean, Stapelfeldt, and Close 1999). These non-detections are almost certainly due to dynamic range limitations of currently available instrumentation. Face-on disks, or young disks in which planetesimal formation has depleted the small scattering grains, are difficult to distinguish from the stellar glare. Thus while current techniques already offer the spatial resolution needed to study young disks, they fall well short of the required dynamic range. By removing this limitation, NGST coronagraphic imaging will make the circumstellar environments of hundreds of young stars accessible to detailed study.

A NGST coronagraph can reveal the structure of protoplanetary disks at radii corresponding to our Solar System's Kuiper Belt. At the distance of the nearest star-forming clouds, NGST's 0.04 arcsec FWHM PSF at $\lambda = 2$ microns corresponds to a spatial resolution of 5 AU. CCM observations can provide direct measurements of disk outer radii and radial brightness profiles. Multicolor imaging will allow a disk's dust properties to be diagnosed, and comparison of the images with scattered light models will allow a disk's scale height and density profile to be derived. These data will lead to a better understanding of the physical conditions in the outer parts of the protoplanetary disk, the formation region of cometary planetesimals. In the more face-on disks, NGST/CCM images will reveal radial structures in the disk mass distribution. These may include inner holes or gaps dynamically induced by stellar or planetary companions, and wakes, density waves, or accretion streams in binary systems. The coronagraph will enable direct imaging of young jovian planets themselves within the disk: a 5 M_J

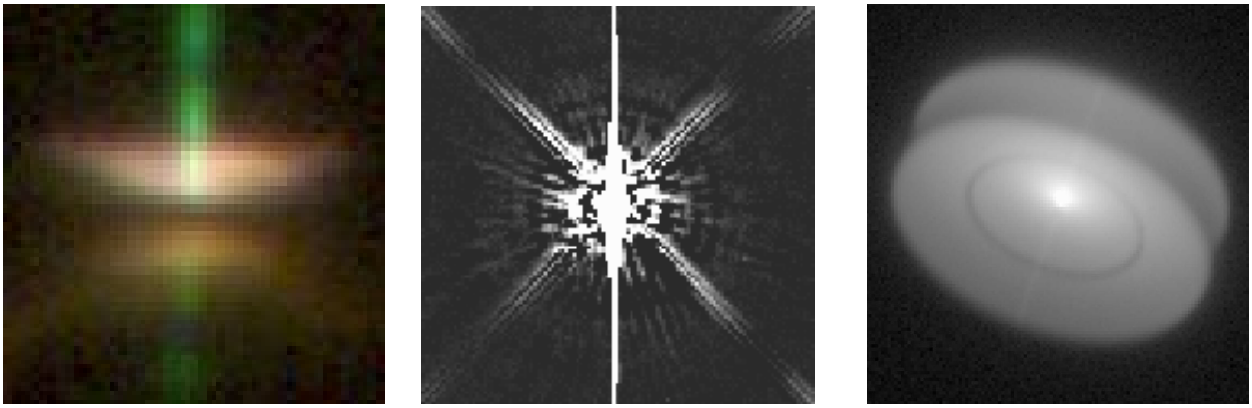

Figure 1-2 *Visibility of YSO circumstellar structure. In the left panel, an edge-on disk serendipitously blocks the glare of the central star in HH 30 as seen by WFPC2/HST in visible light. The HST image in the middle panel shows that even with 10 times the circumstellar mass of HH 30, the glare from the weak-line T Tauri star LkCa 15 totally obscures its circumstellar structure. At right, a model resembling HH 30, at an assumed distance of 140 pc, but rotated from edge-on, shows that a 2000 second CCM exposure in K clearly reveals the disk structure. The model has the same circumstellar mass as HH 30.*

object at age 10 million years presents of a contrast of 10^{-5} versus a central T Tauri star. NGST/CCM can detect all such objects in the nearest star-forming clouds at projected separations of 30 AU or larger.

Sensitive optical imaging with NGST/CCM will track the dispersal of protoplanetary disks by comparative studies of disks around stars of different ages. IRAS measurements suggest that the larger part of the disk mass disperses on timescales of 10 million years, and that the inner regions of the disk are the first to clear (Strom *et al.* 1989). A NGST coronagraphic survey of disks around Classical T Tauri stars, weak-line T Tauri stars, and young cluster stars such as the Hyades could verify this scenario by measuring the disk optical depth, and frequency of inner holes and gaps as a function of stellar age. Short wavelength imaging is a good way to achieve this goal: At $\lambda = 2.0$ microns, the scattering cross-section of interstellar dust is 60 times larger than the dust emissivity at $\lambda = 60$ microns, and 1,000 times greater than the dust emissivity at $\lambda = 1.3$ mm (Beckwith *et al.* 1990). As a result, a uniform surface density disk of radius 100 AU can contain as little as a lunar mass of dust and still be optically thick enough at near-IR wavelengths to produce detectable nebulosity at the distances of the nearby star-forming regions. NGST/CCM images will thus be very sensitive to dust content in dissipating protoplanetary disks. Such a disk evolution study will help to establish the timescales for the settling of dust to the disk mid-plane, the depletion of dust as the grains coagulate into planetesimals, and the final clearing of the initial dust inventory from the system. These disk evolution issues are a specifically recommended investigation in the roadmap of NASA's Origins program.

The youngest stars generally possess collimated bipolar emission line jets which trace high velocity outflows emerging perpendicular to the disk plane. These outflows are thought to arise as a by-product of the accretion process which builds a protostar from the surrounding disk and envelope material. A recent theory suggest that solid material from the disk may be processed through these flows in multiple cycles which could account for the formation of chondrules found in meteorites (Shu, Shang, and Lee 1996). Maps of the physical conditions such as density and temperature within the jets can be made using ratios of images taken in bright emission lines such as 1.87 micron Paschen α, 1.64 micron [Fe II], and 2.12 micron H_2. The collimation mechanism for these jets is uncertain, since measurements of jet properties near the source are made difficult by the glare of the central star. It is particularly important to measure jet widths and opening angles as close to the star as possible, as these define the physical scale of the source region (Ray *et al.* 1996). A NGST coronagraph will make these measure-

ments to within 30 AU of the central engine in dozens of young stars whose jets have been beyond the contrast capability of previous studies.

1.2.3 Debris Disks and Structures

About 15% of main sequence stars are known to possess circumstellar dust to the sensitivity limits of the IRAS survey (Backman and Paresce 1993). These debris disks span four orders of magnitude in dust density, from the tenuous zodiacal light in our own solar system to the disk of Beta Pictoris. In all these systems, the survival timescale for an individual dust grain against the effects of Poynting-Robertson drag is relatively short—only 10^6 to 10^7 years. The presence of such short-lived material around stars long after their original protoplanetary disks have dispersed thus requires the ongoing production of new dust particles by processes such as collisions within planetesimal populations (comets and asteroids) and sublimation of comets during periastron passages. Further, shattering collisions and star-grazing orbits require the presence of planetary-mass perturbers. The mere existence of main sequence debris disks thus indirectly indicates the presence of planets.

Furthermore, the internal structures of debris disks offer an interesting window into the properties of the host planetary system. In our solar system there are irregularities superposed on the general smooth zodiacal dust distribution due to the most recent dust production events such as major collisions and comet passages (Reach 1998). Moreover, there are asymmetries and features produced by the dynamical influence of the planets. For example, our zodi cloud is not centered exactly on the sun, its mid-plane is warped, and Earth has resonantly trapped an enhanced ring of dust in its orbit that includes an extra dense wake directly behind us (Dermott *et al.* 1998). Jupiter has such a resonant ring; the other planets in our solar system may also. Nearby debris disk systems such as Vega, Fomalhaut, and Epsilon Eridani are thought to represent dust produced in analogs of our Kuiper Belt, i.e. reservoirs of planetesimals a few 10s to 100s of AU from their parent stars. Maps of the submillimeter thermal emission from these systems made at 12 arcsec resolution (Holland *et al.* 1998; Greaves *et al.* 1998) reveal large-scale structures in these debris disks which may also indicate the presence of planetary mass perturbers. The Beta Pic disk has several types of asymmetries most easily explained as due to the dynamical influence of planets, including a mid-plane warp that could be caused by a jovian mass with orbit inclined to the disk grains and their parent bodies (Burrows *et al.* 1995). The morphological features of exozodi clouds are thus a key diagnostic that can be used to locate and even estimate the masses of embedded planets.

The prototype debris disk systems are inferred to have central low-density zones that should be filled in quickly by P-R drag unless something, e.g. the shepherding influence of an outermost planet, stops the inward drift of grains. This argument may also apply to many stars with far-IR dust emission discovered by IRAS or ISO but not resolved, having possible central clearings implied by spectral energy distributions (e.g. Dominik 1998). Also, some of the systems (Beta Pic, Fomalhaut) extend to large radii whereas others (Vega, HR 4796) seem to be limited to relatively narrow annuli. The systems with sharp outer boundaries might be showing the dynamical influence of planets or larger companion mass outside the disks. Another possible scenario for indirect planet detection, albeit one requiring further modeling, would be a system like 16 Cyg B in which a large planetary mass has been found in an eccentric orbit near the star. Dynamically forced spiral density waves might appear in a dust cloud around this star, perhaps extending far from the star relative to the location of the perturbing planet.

NGST/CCM will provide a powerful capability to resolve the internal structures of debris disks in reflected light. In comparison to the recent HST/NICMOS results for HR 4796 at 2 microns (Schneider *et al.* 1999), NGST/CCM will allow imaging studies of systems more than an order of magnitude more tenuous, and at three times the spatial resolution. Direct imaging of extrasolar zodi and KB dust structures at high spatial resolution and in numerous distant systems will allow the disks' radial extents, density profiles, central clearings, edges, and major asymmetries to be resolved, providing compelling indirect evidence for planets in such systems. To date, only the two densest debris disks (Beta Pic and HR 4796) have been detectable in scattered light at the low contrast levels which have been accessible at near-IR wavelengths. Our optical simulations indicate that

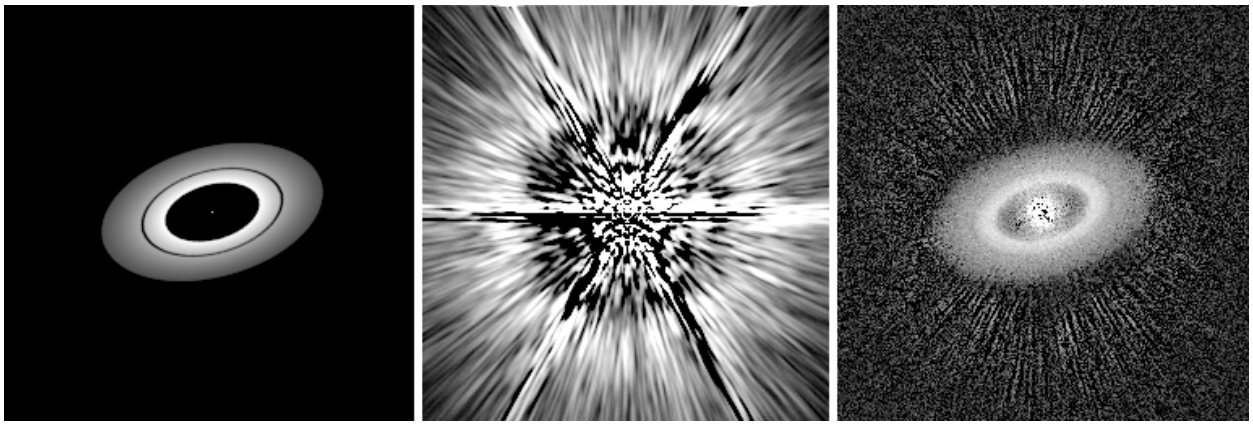

Figure 1-3 *Simulation of a Fomalhaut-type debris disk imaged with NGST. Shown at left is the model 500 zody disk at a distance of 50 pc, with material distributed between radii of 30-70 AU and viewed 35 degrees from face-on. The next two panels simulate PSF-subtracted one hour exposures with NGST in K band for a solar-type star at this distance (K= 8). Without a coronagraph, NGST would obtain the image shown in the center panel, where the faint light of the disk is overwhelmed by PSF subtraction residuals. Using the proposed Coronagraphic Camera Module (CCM), however, NGST would obtain the image shown at right. The direct stellar glare is suppressed and the debris disk (including a radial gap 2 AU in width) is clearly seen. All images are shown in log stretch.*

Kuiper debris disk systems with dust optical depths of a few times 10^{-5} (similar to that of Fomalhaut, or a few hundred times that of the Zodiacal cloud) will be accessible to NGST/CCM in a few hours of integration time. Initial estimates from IRAS detection statistics imply that hundreds of such targets with spectral types A–K are available within 60 pc of the Sun.

1.2.4 Near-Environment of AGB and Post-AGB Stars

The mass-loss processes that accompany late stellar evolution are responsible for the enrichment of the ISM with the products of nucleosynthesis, another aspect of NASA's Origins program. The circumstellar envelopes of dying stars contain the key to understanding the mass ejection which generate proto-planetary and planetary nebulae (PPNe & PNe). All stars in the 1–8 $M_\odot$ mass range eject half or more of their initial mass during the last few 10^4 years of AGB evolution and produce PNe. More massive stars also lose mass at comparable rates during a supergiant phase just before ending their lives as Type II supernovae. Yet, the process of mass-loss in these objects remains very poorly understood because the near-stellar environment (NSE) within about 100 stellar radii (1 stellar radius ≈ 2–4 AU) is virtually unexplored. It has not been possible to study detailed structures in the NSE because these are typically fainter than the glare of the bright central star by many orders of magnitude. Roughly, $F/S \sim 10^{6-8} (\lambda / 2\mu m)^4 \{(\phi / 2'')(V_e/10 \text{ km s}^{-1})(D/500 \text{ pc})\}^3$ arcsec^2 for spherically-symmetric mass loss at rates $\dot{M} \approx 10^{-6}$–10^{-8} $M_\odot$ yr^{-1}, where S = NSE surface brightness at offset ϕ from star, F = stellar flux, V_e = outflow velocity and D = distance. Red giant and supergiant stars are quite bright at infrared wavelengths, with K-magnitudes $\lesssim$ (-1 to 2) at D $\lesssim$ 1 kpc, since they typically radiate ~10^4–10^5 $L_\odot$ at T_{eff} ~(2000–3000 K).

CCM provides the combination of high-contrast imaging and sensitivity necessary to study NSEs. Observations will be made in the light of the dust-scattered stellar continuum radiation and the spectral lines of neutral and ionized gas. Multicolor imaging will be used to study the 3-D geometry of the NSE, determine the location and number of illuminating sources, and the properties of the dust. A variety of low-to-high excitation states of the gas can be probed with spectral lines available in the NIR, including H_2 (2.12 μm), Paschen α (1.87 μm), Brγ (2.16 μm), and [FeII] (1.64 μm). The 2.1 μm v = 1-0 *S* (1) H_2 and the 1.64 μm [FeII] lines have proven to be particularly useful for probing shocked gas. Recent HST

(Hora *et al.* 1999) and ground-based observations (Welch *et al.* 1999) of the very young PN, Hb12, have revealed new complex internal geometrical structures such as multiple elliptical rings and hourglass bubbles close to the central star. Although the origin of such structures remains unknown, it probably involves the interaction of fast collimated stellar winds with ambient circumstellar material in the NSE, which can only be probed with an instrument like CCM. Using a broad K-band filter, CCM will be capable of imaging the NSE at $\phi = 1.5''$, with a signal-to-noise ratio of 5 at 0.07″ resolution, for a star with $\dot{M} = 2.3 \times 10^{-7}\ M_{\odot} yr^{-1}$ and K-magnitude of 1 in 15 minutes. The solar neighborhood within 1 kpc contains about 50 bright red giant stars with $\dot{M} > 10^{-6}\ M_{\odot}\ yr^{-1}$ (Jura & Kleinmann 1989) and several hundred more with mass-loss rates $> 10^{-7}\ M_{\odot}\ yr^{-1}$. Thus, CCM's ability to routinely image the region of stellar wind acceleration (20–200 R_*) in several hundred AGB red giants/supergiants within 100–1000 pc will provide a representative sampling of the ubiquitous mass-loss phenomenon, providing answers to the such critical questions as whether the mass-loss is spherically symmetric, smooth or clumpy, continuous or episodic.

The NSE discovery potential of coronagraphy is demonstrated by a serendipitous "astrophysical coronagraph" in the form of an edge-on dusty disk blocking the direct light from the central star in the bipolar reflection nebula CRL2688. Thanks to this rare geometry, near-infrared and visible images from NICMOS & WFPC2 (on HST) revealed twin jet-like structures and multiple arcs within 2″–5″ of the central star (Sahai *et al.* 1998a, 1998b). Polarimetric imaging at 2 μm led to the discovery of a faint red embedded companion, and the precise location of the invisible central star. Unfortunately, the favorable geometry of CRL2688 is not available for most mass-losing stars. Even objects (such as the PPN M1-92) where the disk is slightly more inclined (or less optically thick), the glare of the visible central star hides structure close to it (Fig. 1-4; Sahai *et al.* 1999, in preparation). Thus, in spite of the contrast advantage afforded by imaging line emission, the structure of the shocked gas near the star (crucial for probing the unknown physical mechanism responsible for the transition from spherical to aspherical mass-loss in dying stars), cannot be seen in M1-92. Similarly, the irregular circumstellar structure of the prototype Mira variable o Ceti, suggested by interferometric observations at 11 μm (Lopez *et al.* 1997), is completely obscured by the light of the visible star in HST images. CCM imaging of o Ceti and similar objects can directly distinguish among the range of possible models allowed by the interferometric data (a disk, spherical shell with a few clumps, or a set of thin partial shells at $\phi = (0.3''–1.2'')$, and reveal mass-flows due to the hypothesized accretion of the red giant wind by its companion. Similarly, for the symbiotic Mira RX Pup, even though an intriguing one-sided jetlike emission feature has been found at $\phi > 1.3''$ from ground-based coronagraphic observations (Paresce 1990), much of the light seen in this

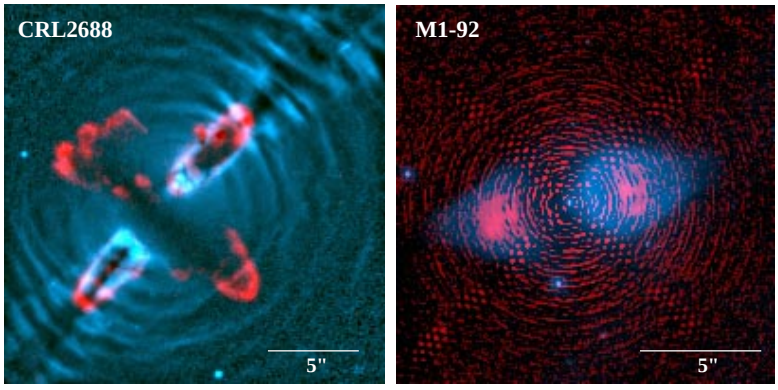

Figure 1-4 *HST near-infrared (red) and visible light (cyan) images of CRL2688 and M1-92, two dying stars expelling material into the ISM. In CRL2688, the rich structure in the near stellar environment can be seen because a fortuitous edge-on disk of dust completely obscures the central star. The NIR images show emission from shocked gas in the 2.1 μm H_2 line. The dramatically different geometry of this emission compared to the scattered light seen in the visible requires new theoretical models for the mass-loss processes. In contrast, the disk in M1-92 is less edge-on than CRL2688 and the glare of the central star in this PSF-subtracted image obscures the details of its mass-loss structure. CCM will allow high contrast imaging of this region in several hundred dying stars free of disk orientation selection effects.*

image is starlight scattered by the atmosphere and telescope. The capability of CCM is needed in order to probe the origin of such jets in symbiotic stars close to the star, and to obtain accurate morphological/photometric information.

New science enabled by CCM includes (1) the direct detection of hypothesized "holes" in the NSE where the mass-loss rate is thought to have decreased in the past ~10^2–10^3 years in various classes of AGB/post-AGB stars, including high-latitude supergiants (Hrivnak *et al.* 1989), RV Tauri stars (Alcolea & Bujarrabal 1991; Jura 1986), optically visible carbon stars (C/O abundance ratio >1) and S-type (C/O~1) stars (Chan & Kwok 1988), (2) investigations of episodic mass ejections, accretion, and jet formation which characterize symbiotic stars (e.g. Paresce & Hack 1994), and (3) studying the poorly understood transition of round AGB red giant envelopes into aspherical PNe by detecting disks, jets, and companions, all of which have been directly or indirectly implicated in the formation and evolution of aspherical PNe (e.g. Soker & Livio 1994; Soker 1996).

1.2.5 QSO Origins and Host Galaxies

The remarkable commonality between the history of QSOs and the star formation rate in the universe compels us to search for common physical mechanisms which govern the formation and evolution of QSOs and their host galaxies. Do QSOs form as a natural consequence of mergers or starburst activity in the cores of protogalaxies? Is there a threshold for the local density of protogalaxies which must be met to trigger the formation of massive black holes? What did galaxies look like as they formed the earliest QSOs? To answer these questions, we must travel back to a time when both QSOs and galaxies are forming, redshifts greater than ~ 2, and compare the environments we see with NGST to those detected around low redshift objects.

For example, there is a substantial body of evidence at low and moderate redshifts (and some theoretical and numerical justification for the belief) that galaxy mergers and interactions are largely responsible for the fueling of AGN activity. Such phenomena should be both more frequent and more spectacular during the early stages of galaxy formation and evolution, and in particular near the peak merging epoch, believed to be around the redshifts of 2 to 3 (see, e.g., Baugh *et al.* 1998). It is probably not a coincidence that the comoving density of quasars peaks at the same redshifts (Hartwick and Schade 1990, and references therein). Yet, at the present there is practically nothing known about the host galaxies and immediate environments of quasars at such redshifts. This is a purely observational limitation: the scattered QSO light greatly outshines their host galaxies and close companions. HCOS would be an ideal instrument to tackle this problem, and uncover for the first time the host galaxy structures at the time when quasars were at their peak.

On the other hand, other mechanisms have been proposed for fueling of AGN at lower redshifts, e.g., inflow on radial orbits in galactic bars, cooling flows in clusters and massive ellipticals, and so on. Such mechanisms may indeed be operating in at least some cases at lower redshifts, but may be uncommon at the earlier epochs, since they require dynamically evolved (bars) or virialized (cooling flows) structures which may not yet be in place. By comparing images of circum-quasar regions at a range of redshifts NGST may be able to probe the evolution of QSO fueling mechanisms as a function of redshift and large-scale environment, radio loudness, etc.

Adequate imaging of QSO hosts and environments at very modest redshifts (a few tenths) can be already accomplished with the HST (and obviously the NGST) using simple imaging and PSF subtraction techniques (e.g., Bahcall *et al.* 1997). However, a more sophisticated approach would be necessary to do an equivalent experiment at the peak of the QSO era, at z > 2 or so. We also note that even for the low and moderate redshifts, CCM imaging of QSO hosts would reveal structures at smaller separations from the nucleus than is possible with the simple PSF subtraction, e.g., small-scale bars, circumnuclear starbursts, etc.

QSOs probably mark the sites of the earliest galaxy formation. A generic expectation in most models of galaxy formation, including the standard CDM cosmogony, is that the first galaxy-scale objects will be forming at the highest peaks of the primordial density field, which itself would be strongly clustered *ab initio* (Kaiser 1984; Efstathiou & Rees 1988). Some of the first massive protogalaxies may be the hosts of quasars at $z > 4$, undergoing an early quasar phase while forming the bulk of their stars, in a still-collapsing protogalactic

structure (Haehnelt & Rees 1993). These fields can be naturally interpreted as the cores of future rich clusters. Central starbursts may be triggered in forming galaxies by mergers and interactions with subunits, and may fuel a young black hole via supernova-induced viscosity in the starburst ring and dissipation in merging gas flows.

The combination of the light gathering power of NGST and the exceptional image contrast of CCM are required to determine the nature of QSO host galaxies, the incidence of merging and starburst activity, and the nature and frequency of companions at high redshift. This is because the host galaxy itself will be faint, complex, and heavily attenuated by Tolman dimming. CCM provides sensitivity for $z \sim 4$ and QSO/galaxy luminosity ratios of 100 to local star formation activity greater than $1 M_{\odot}/yr/kpc^2$ (typical for local starbursts) at radii greater than 1kpc. We show in Figure 1-5 that such a galaxy can only be detected using CCM to suppress the QSO scattering wings to achieve a contrast ratio of $>3 \times 10^4$ at angles greater than 0.1–0.3″. This in combination with a NIR detector is ideal for searching for central starburst activity using emission lines and redshifted UV stellar continuum light. CCM provides access to star-forming clusters in the host galaxy and to the morphology of the nuclear environment, reaching in as near as 100 pc from the core. It is important to image in close since here the dynamical times become comparable to the age of the QSO, making a causal connection possible.

1.3 Historical Setting for CCM

The scientific case for a mission like CCM is an inevitable outgrowth of the stunning success of the Hubble Space Telescope (HST) science programs. HST has begun the exploration of the universe with spatial resolution that is unavailable at ground based observatories at visible wavelengths. CCM is a direct extension of HST science to a discovery space that HST will never penetrate—the nearest few arcseconds of stars and quasars for faint objects and structures which are of fundamental importance to NASA's Origins program.

1.3.1 Hubble Space Telescope

The capabilities and limitations of HST for direct imaging near bright objects are well understood (Brown & Burrows 1990), and examples drawn from existing science programs have been discussed in earlier sections of this report. Three current or future HST instruments offer partial forms of coronagraphy. None of them provide correction of the surface figure errors on the Hubble primary mirror beyond the large (low order) correction for spherical aberration (SA). The

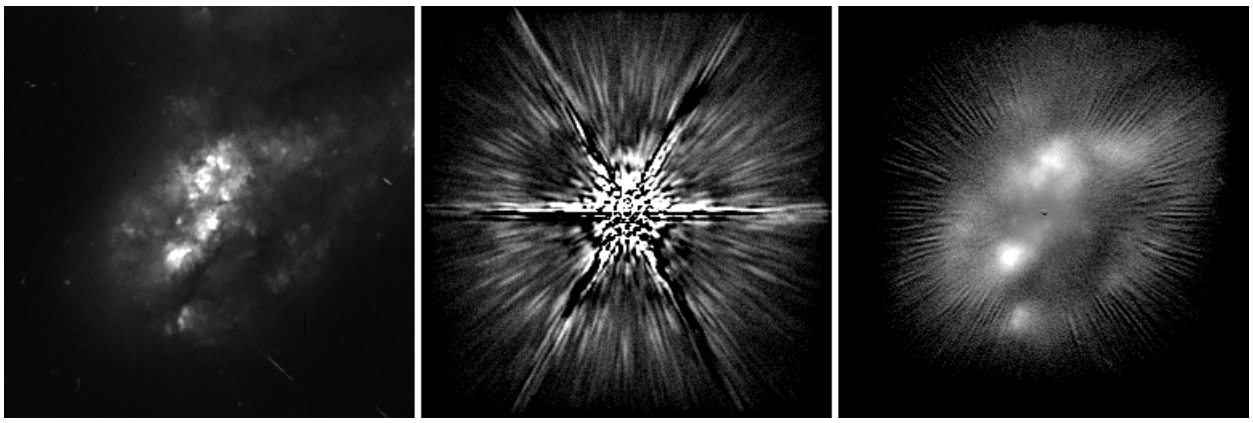

Figure 1-5 *A QSO host galaxy, as it would appear to NGST in a 2000 second exposure at 2 μm. An HST image of NGC 7592, a Seyfert 2 galaxy at z = 0.027, was first doubled in physical dimensions to simulate a massive galaxy fueling a QSO engine, then moved to z = 2 by appropriately reducing its surface brightness and apparent diameter. The left panel shows the QSO/galaxy as it would appear with 0.026 arcsecond pixels with no diffraction. The magnitude 20 QSO, which is 10x more luminous than the entire surrounding galaxy, is completely contained within the central pixel. The center panel is a direct NGST image, PSF-subtracted to reduce the central glare. The panel at right is the same observation with CCM.*

NICMOS camera 2 includes a coronagraphic hole and utilizes its internal cold pupil stop as a Lyot mask. This system became misaligned by the NICMOS dewar thermal anomaly after it was installed in HST. Available NICMOS PSFs exhibit a point source contrast limited to about 10 magnitudes at 1.5″ separation from a bright star (Krist *et al.* 1998), which is insufficient to detect brown dwarfs like GL 229B inside a 10 AU radius of most stars within 10 pc. The STIS instrument contains an occulting bar in its focal plane and a partial Lyot stop that does not mask diffraction from the HST secondary obscuration and support spiders. The STIS coronagraph improves contrast by preventing saturation and blooming on the CCD detector, but again offers only an order of magnitude contrast improvement. Finally, the ACS/ABC, currently scheduled for installation in March 2001, will include an occulting mask that is located in the spherically aberrated image plane, prior to its internal correction for the SA error on HST's primary mirror. This system includes a full Lyot stop to reduce diffraction from the HST secondary spiders and primary mirror edges, but since its occulting spot is in the aberrated beam, a significant fraction of the starlight skirts around the spot and into the surrounding background. The ACS/ABC is expected to reduce background within the first few arcseconds of the star by about an order of magnitude. Simulations of the ACS/ABC performance indicate that it will not be capable of detecting exoplanets, and that most young stellar object disks will be completely obscured behind its large occulting spot. In summary, all of the existing or planned HST instruments suffer from significant limitations in their coronagraphic imaging modes, and none fulfill the full potential of space-based coronagraphic imaging.

1.3.2 Results from SIRTF and SOFIA

The launch of the SIRTF observatory in 2001 will make an important new tool available for debris disk studies. The photometric sensitivity of SIRTF should allow thousands of these systems to be detected. In cases where exozodiacal infrared emission is not spatially resolved from its central star, SIRTF's sensitivity limit will be determined by how well excess emission can be discriminated from the photosphere. This detection limit corresponds to about 10 zodies for a K star—better than what CCM will achieve. SIRTF's thermal infrared spectroscopic capability will permit studies of grain properties in these disks. However, SIRTF's sensitivity to these objects is not matched by its spatial resolving power. At its limiting resolution of 5″, SIRTF will be able to map less than 100 of the nearest debris disks systems (Werner 1998). The SOFIA observatory will offer somewhat better resolution (1″) but with less sensitivity. CCM images will provide 0.04″ resolution on systems with $\tau = 10^{-5}$ (10 zodies) or brighter within 60 pc. CCM offers the most effective way to study small-scale disk internal structures which indirectly betray the presence of planets, and can do so in a large number of exozodiacal systems. SIRTF data will be of great value in selecting target objects for high resolution imaging. CCM will build on the success of SIRTF to extend our understanding of dynamical processes in the remnant disks of main sequence stars.

1.3.3 Astrometric and Radial Velocity Planet Searches

CCM investigations of nearby planetary systems will create a revolutionary new knowledge base that will complement and significantly augment other planet-finding programs. Current groundbased radial velocity and astrometric surveys, as well as future high-precision space astrometry with the Space Interferometry Mission (SIM) will provide mass and period information for planets. These missions observe the motion of the central star around the barycenter of its system over times comparable to the orbital periods of the planets. They provide mass and orbital radius of the planets through this indirect effect, but do not provide photons from the planets themselves. CCM provides direct access to a giant planet's thermal emission, giving photometric and color discrimination of the planets and their atmospheres. In particular, CCM observations of nearby planetary systems are complimentary to SIM, providing confirmation of planetary orbital parameters.

Starting with the two-telescope Keck interferometer in the year 2000, astrometric surveys will begin to make important contributions to extrasolar planet searches. The fulfillment of astrometry's potential will come when sensitive, multi-baseline, ground-based optical/near-IR interferometers become available (in the case of Keck, sometime around 2002), and with the launch of SIM in 2006. The Keck

interferometer will have the sensitivity to detect the gravitational influence of planetary companions similar to Uranus circling hundreds of nearby stars, while SIM may even achieve the indirect detection of Earth mass objects. Both astrometric interferometers are expected to be in operation during the period of the CCM primary mission. The simultaneous availability of astrometric indirect planet detection and high contrast direct imaging would be a tremendously effective combination for study of substellar objects. CCM will be capable of detecting jovian planets with only a few hours of observing toward targets within 8 pc, whereas astrometric surveys will require several years of measurements to establish their detections. Mass determinations from astrometry can be combined with radius values obtained by CCM to derive the planet's mean density—a fundamental physical parameter. The direct imaging and astrometry techniques can thus reinforce each other, confirming the other's results. Early results from Keck may be available to identify specific stars for deep imaging with CCM, and to suggest optimum observing windows when exoplanets would be seen near elongation. CCM will be available for immediate follow-up of planets and brown dwarfs detected by its contemporary astrometry missions, and will be the only available means for obtaining essential photometric characterization of these objects.

1.3.4 Large Ground-based and Balloon Telescopes with Adaptive Optics

A scheme for direct exoplanet detections using large ground-based telescopes is discussed by Angel (1994). To detect Jovian planets in their near-infrared reflected light, such observations must achieve contrast levels of one billion. High-order adaptive optical correction of atmospheric phase and intensity deviations will be required, at 10,000 or more locations across the entrance pupil at rates of 2 kHz or higher. The tight PSF from a large telescope aperture, and multiple observations of each star with a variety of telescope orientations must be used to minimize diffraction effects, and although not elaborated by Angel (1994), additional measures would be required to reduce systematic sources of stray light to levels commensurate with the adaptive correction of scattered light. This might include the control of diffracted light due to telescope structures with a coronagraph or the use of a deep nulling technique. The technology path for ground-based systems adequate for a planet search will be the subject of research for some time to come. The need for high S/N in the fast, real-time AO control loop would appear to restrict such techniques to relatively bright stars.

To a suitably equipped NGST, the task of direct exoplanet detection is much easier. A critical advantage is the space observatory's access to the 4.8 micron band, where jovian planets and brown dwarfs appear hundreds of times brighter than in the near-infrared. At this crucial wavelength, the huge sky backgrounds that groundbased telescopes must contend with ($M = 10$ mag arcsec^{-2}) will prevent them from making sensitive observations to the absolute $19 < M < 24$ range characteristic of mature Jovian planets. Direct detection programs from the ground are thus forced to confront the much less favorable contrast requirements for observing between 1-2 microns. At 5 microns, the relaxed contrast requirement significantly reduces the need for precision wavefront control, and allowing NGST/CCM to robustly achieve exoplanet detections with the baseline NGST optical configuration. In addition, it will be easier for NGST to achieve its wavefront control requirements than for a groundbased telescope pursuing direct exoplanet detections. In space, a telescope enjoys a far more stable thermal environment and it will not have to contend with the sensing and correction of large atmospheric seeing effects to extraordinary accuracies at kilohertz rates.

New balloon technologies suggest that long duration flights of an HST-class telescope at altitudes as high as 35 km will become possible in the next decade. An in situ characterization of atmospheric seeing from a high-altitude balloon platform is the subject of a proposed NASA study that will ultimately provide a description of the spatial and temporal wavefront errors to be expected. It is anticipated that real-time wavefront sensing and correction would be required to meet the optical scatter requirements for direct planet imaging, again suggesting that the technique will be restricted to bright stars.

1.3.5 Space-based Nulling Interferometry

The Terrestrial Planet Finder (Beichman, 1996) is a concept for multiple-aperture cophased imaging of faint point objects against

the glare of nearby parent stars. TPF is technically feasible with 10 μm IR long-baseline interferometric nulling techniques. While challenging, the critical enabling technologies have been identified and the engineering implementation is under study. It is important to note that a sparsely-filled-aperture telescope, such as TPF, provides ambiguous information when presented with a complex image, and there is considerable uncertainty about background complexity in a TPF discovery field. This is due to the likely presence of non-planetary objects, including remnant debris disks, extrasolar comets, luminous companions, low-contrast confusion-limited background galaxies, and even Zodiacal background from within our solar system. Observation of these structures over a representative population of candidate systems is a fundamental first step to understanding the evolution of planetary systems, yet virtually all of these phenomena lie well beyond the observational capabilities currently available to astronomy.

Taking the viewpoint that the roadmap to discovery of earth-like planets orbiting nearby stars is best covered in incremental steps towards the ultimate goals of TPF, then an important preliminary step is the imaging of candidate systems with a large filled-aperture telescope. CCM would provide clear discrimination between all classes of objects listed above, a task that would pave the way for a TPF based on nulling interferometry. Planetary systems discovered and characterized by CCM will provide the knowledge base needed to optimize the TPF design and select suitable candidate systems for further investigation.

2. ENGINEERING

2.1 Design Concept

CCM is a coronagraphic camera concept for NGST. A coronagraphic camera is distinguished from a generic imaging instrument by the addition of two essential elements—an occulting mask in the focal plane to attenuate the light from a bright unresolved central object, and a Lyot mask at a subsequent pupil plane to attenuate diffracted light that has bypassed the occulting mask. A telescope with coronagraphic camera is one of several technologies that have been considered for high-contrast imaging in future space astronomy missions. NGST provides active wavefront correction in its yardstick design, and the ISIM provides the ideal setting for a coronagraphic camera. Other approaches that have been reported recently include various combinations of interferometric deep nulling, multi-aperture telescope arrays, active wavefront correction, aggressive pupil apodization, and dark speckle processing (Angel and Woolf 1997; Beichman *et al.* 1999; Moutou *et al.* 1998; Rabbia *et al.* 1998; Woolf and Angel 1998).

CCM will use a 1×1 arcminute patch of sky located at one of the extreme corners of the shared NGST focal plane (Fig. 2-1). The CCM utilizes a pickoff mirror that extends from one end of its truss structure, capturing its small area of the focal plane and diverting the beam into an optical system that is spaced well away from the shared focal plane area. The CCM uses 2.5% of the focal plane area and its structure consumes approximately 2.5% of the volume of the yardstick ISIM enclosure. CCM therefore has minimal impact on the design and packaging of the ISIM instrument complement.

2.1.1 ISIM Environment

We begin with an accounting of the elements of the ISIM environment that are provided by the NGST project. These elements are defined in the NGST report format specification (http://ngst.gsfc.nasa.gov/cgi-bin/pub-download?Id=266) and by other public documents and clarifying conversations with M. Greenhouse.

The yardstick NGST and ISIM structures will project a wavefront-corrected and jitter-stabilized optical beam to a shared focal plane

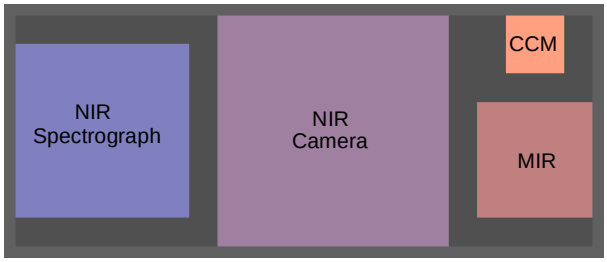

Figure 2-1 *NGST focal plane, showing the location of the CCM 1×1 arcminute field of view.*

area within the ISIM structure. The optical wavefront is corrected to a nominal lambda/14 rms (diffraction limited) at 2 microns wavelength. The focal plane area measures 10×4 arcminutes on the sky. Telescope pointing will be stabilized to 0.0027 arcseconds rms by one or more fine steering mirrors (FSMs). ISIM shrouds and structural members will be passively cooled to 35 Kelvins. A generic detector front-end is provided. We assume this detector front-end includes either an Insb or HgCdTe 2048×2048 array with 18 μm pixels and long wavelength sensitivity cutoff at 5.5 μm, together with separate readout electronics, data system, and instrument control processor that resides in a warm bay external to the ISIM enclosure.

Here we have assumed a seven-hexagon segmented primary mirror configuration (specifically a TRW design for NGST with 9m aperture edge-to-edge). We have modeled other proposed segmentation schemes in detail, including the GSFC yardstick with eight deployed "petals", and a Lockheed concept displayed at the June 1999 AAS meeting with an overall circular outline mirror and eight "keystone" segments (Fig. 2-2). The CCM concept favors a primary mirror with a small number of large segments over other designs, such as the 36-hexagon BASD telescope, with a large number of smaller segments. This is because the edges of each mirror segment introduce additional diffraction, surface figure rolloff, and wavefront phase discontinuities that must be masked at the CCM Lyot stop. The large-segment telescope characteristics listed above result in nearly identical science performance for CCM, and we use the TRW example to predict

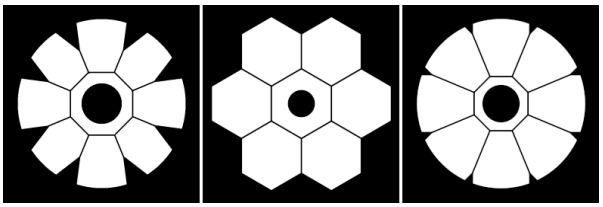

Figure 2-2 *Representative NGST primary mirror geometries.*

performance characteristics that are representative of any of these large-segment designs.

On the other hand, the performance of a coronagraph is very sensitive to optical wavefront errors arising from surface finish on the NGST primary mirror. Surface figure errors with wavelengths in the range of 3–60 cycles across the 8-meter primary mirror will scatter starlight into the nearest few arcseconds from the star. Control of surface figure errors in this spatial-frequency range are both critical to the unique CCM science program and generally outside the traditional specifications of surface figure. Much of the CCM design concept hinges on a detailed description of the NGST optical wavefront, hence much of the concept study has been devoted to understanding the elements of the NGST optical specification that are most critical to the coronagraph performance and the enabled science program. This is discussed further in Section 2.1.10.

2.1.2 Optomechanical Design

A conservative optomechanical design approach is proposed. The coronagraph backbone must be dimensionally stable over time, loading, and temperature, in order to maintain the coronagraph optical alignment. This backbone is a classic truss which surrounds the optics and sensors. It is attached kinematically to the NGST structure near the ISIM focal plane. High flexural rigidity and low mass are implicit to the truss approach.

The system may be regarded as an assembly of two main sections, the coronagraph and the camera. Referring to Figure 2-3, the coronagraph section includes the following elements: a flat pickoff mirror M1, a graded density occulting spot S, and a toroidal-figured mirror M2 that creates a high quality pupil image at the plane of the Lyot mask L. The camera section includes a flat fold mirror M3 which is tip/tilt articulated for image dithering, a three-mirror anastigmat A1/A2/A3 relay, and a filter wheel assembly (FWA), all followed by the focal plane detector array. The composite truss structure carries both sections, but for ease of integration, the camera is integrated on a separate substructure of the same low expansion material. The camera substructure facilitates alignment of the sensitive camera optics prior to integration into the instrument. Schott Zerodur is selected as the mirror substrate material because of its excellent thermal expansion match to the mechanical structure and its compatibility with optical finishing processes. The optics in the coronagraph section, while not as challenging to align as the camera, nevertheless require highly efficient baffling against stray light, and provisions to maintain cleanliness. Each of these is operated at 35K nominal temperature.

In addition, there is a separate electronics chassis, mounted in the warm section of the ISIM, providing drivers and power for the detector array, mechanisms, and the signal interface.

2.1.3 CCM Optical Design

The CCM coronagraph design uses four aspheric mirrors to create a light path that includes two pupil images and two stellar images. The first pupil image is well corrected for effective use of the Lyot stop, while the second provides an optimal position for the filter elements and also provides for additional stray light control. An occulting spot is located in the focal plane of the telescope. This is accomplished by placing the flat pickoff mirror ahead of the shared focal plane, a geometry made possible by placement of the CCM field of view in the extreme corner of the shared focal plane, and ahead of the four mirror system. Of the two stellar images created within the internal CCM optical path, one is intermediate in the light path, while the other is at the detector focal plane.

The optical path, starting at the pickoff mirror, begins with the telescope focal surface, where the occulting spot is placed. A 154 mm diameter torodial mirror then creates a relayed pupil image, where the Lyot stop is located. The intermediate stellar image is then formed, which is relayed through a three mirror, unobscured, decentered aperture camera (with mirror diameters of 182, 58, and 114 mm respectively). A final pupil image exists approximately 175 mm before the detector focal plane, providing a location for the filter

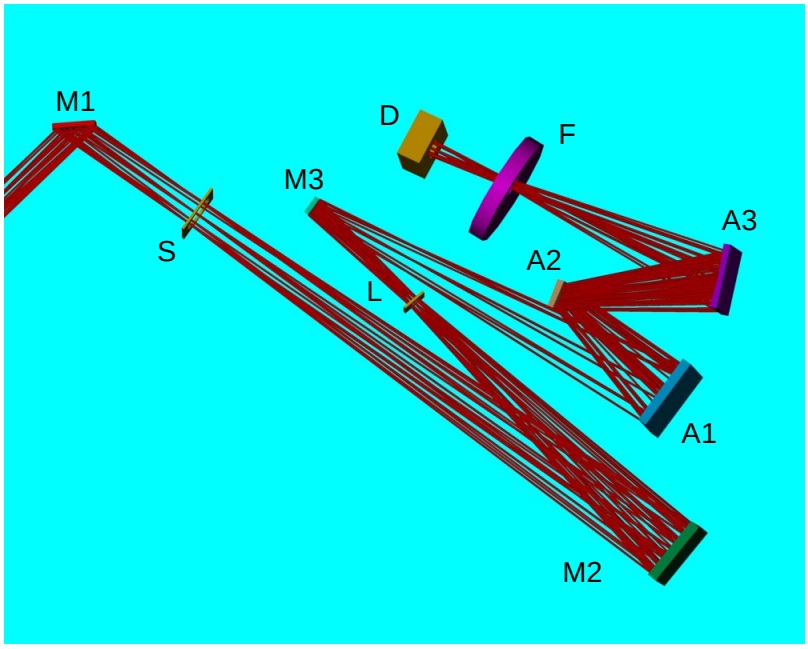

Figure 2-3 *CCM optical path. Pick-off mirror M1, positioned at the extreme corner of the ISIM field of view, directs the light to the coronagraph optics. Occulting mask S, toroidal mirror M2, and Lyot-mask L comprise the coronagraph. Fold-mirror M3 directs the beam to a 3-mirror anastigmat A1/A2/A3 which creates an image at the focal plane array D. Filter-wheel F provides science and calibration elements.*

wheel assembly and additional stray light control. The camera forms the final f/18 stellar image to provide critical sampling at 2 microns wavelength with plate scale of 0.0258 arcsecs per 18-micron pixel. The Strehl ratio at 2 microns is better than 0.75 everywhere over a 37 arcsec diameter field, and better than 0.84 over the central 26 arcsec diameter field.

2.1.4 Structure Volume and Mass

The CCM optics, detectors and devices are mounted within a prism shaped truss (Fig. 2-4), with a beam carrying the pick-off mirror to the NGST focal plane area. This structure consumes a volume of about 0.45 m^3, or approximately 2.5% of the ISIM volume. The truss prism measures 0.90 m at the base, 0.80m in height, and 1.25m in length. The component inventory and mass allocations in Table 2-1 indicate that CCM will be a 53kg instrument, including a 15% mass reserve.

In addition, “warm” electronics, including radiation shielding of critical electronics, is estimated to have a mass of 8kg, bringing the total system mass to 61kg. It is assumed that suitably conditioned power shall be provided to the instrument, and that DC power converters are not required. It is also assumed that NGST will have central processing that will accommodate data and commands, and provide for data compression and telemetry. The warm boxes will include field programmable gate arrays to handle routine functions derived from commands from NGST’s central microprocessors.

Table 2-1. CCM Mass Allocation (kg)

Metering structure		18.6
Composite structure	14.6	
Invar fittings	4.0	
Coronagraph		11.1
Pickoff mirror assembly	2.4	
Fore optics baffles and box	3.0	
Occulting disk assembly	0.7	
Reimaging mirror	1.1	
Mirror bipods and mounts	1.2	
Lyot Filter (with xy motors)	1.1	
Fasteners and Invar fixtures	1.6	
Camera		16.3
Aft optics bench	2.6	
Aft optics baffles and box	1.4	
Fold mirror	0.5	
TMA Mirrors	2.1	
Mirror bipods and mounts	1.8	
Filter wheel assembly	1.4	
Thermal straps	1.8	
Detector assembly	2.3	
Cabling (power, signals)	0.9	
Fasteners and Invar fixtures	1.5	
Mass reserve		7.0
TOTAL		53.0

There are threats to add mass. For example, should detectors or radiation sensitive devices be placed at the outer part of the ISIM, they would not enjoy radiation shielding of the outer assemblies, and additional shielding

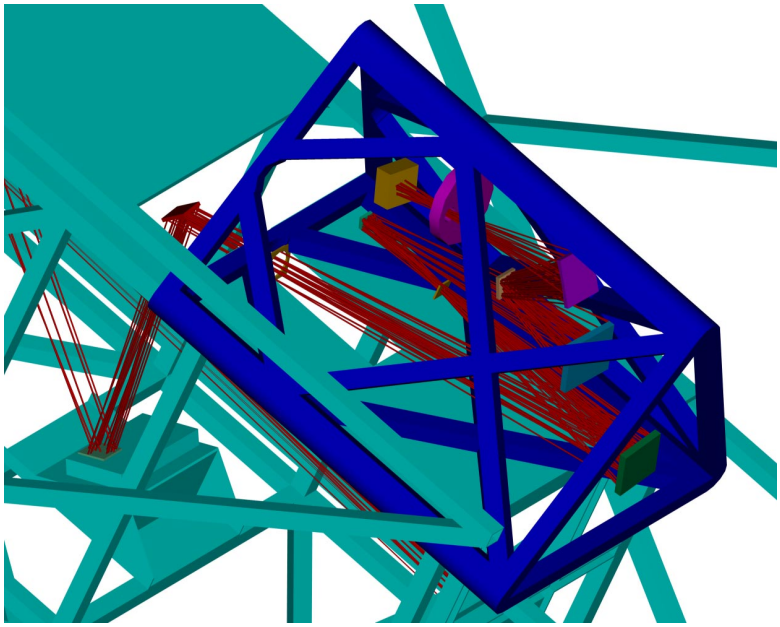

Figure 2-4 *CCM truss (in blue) and essential optical components are shown attached to the ISIM yardstick backbone structure (in green). Zerodur optics and cyanate ester composite truss provide an instrument that can be aligned at room temperature and operated at 35 Kelvins.*

might be anticipated. It is extremely doubtful that more than an additional 6kg of mass would be needed to meet the environmental conditions at L2.

The CCM structure has a packing density of approximately 120 kg/m^3. The packing density is therefore very low, with much of the volume devoted to optical path and free space. Such a low packing ratio may not relate to parametric cost models based on moderate to high packing density. In addition, this low packing density indicates that considerable reductions in the dimensions of the truss are possible if needed to accommodate the integration of other instruments in the overall ISIM design.

2.1.5 Passive Athermalization

The ISIM will be maintained at a uniform temperature near 35K, so questions of operational transient response and gradients do not drive material selection. However, we recognize that the optical paths are fairly long, and some alignments are critical. For example, it is recognized that the three mirror A1/A2/A3 relay camera optics are relatively fast, and performance is expected to be unusually sensitive to dimensional perturbations. These perturbations include the classic optical effects of despace, decenter, tilt, and radius of curvature changes associated with each mirror, all of which can result from material response to temperature change.

Assembly, integration, and test are all simplified if the settings at room temperature are also valid at the 35K operational temperature. This is satisfied either if the materials have zero thermal expansion over the temperature range, or if all materials have a common expansion over the temperature range. A monometallic (metering and optics) aluminum approach was considered, but rejected. Aluminum cannot be finished to the smoothness needed for the optics. Similarly, uncoated beryllium cannot offer the low scatter surfaces needed and nickel-coated beryllium optics will deform with temperature change. Silicon carbide might meet the requirements, but risks associated with this size and class of an instrument. We found no single material that could satisfy the optical and metering requirements.

For CCM we adopt an attractive approach using composites. M55J carbon fiber in a 954-3 cyanate ester matrix provides a dimensionally stable isotropic material with low density (~ 1.7g/cm^3) and moderately high modulus (~ 10N/m^2). It has a near-zero thermal expansion coefficient, and as demonstrated by COI, in plated form it can be matched to the expansion of Zerodur mirror substrates very accurately at both ends of the temperature range. Figure 2-5 (adapted from Dodson *et al.* 1999) illustrates a nearly perfect match at ambient and 35K. Thermal strain is near zero at both laboratory and operational temperatures, and at no temperature is an

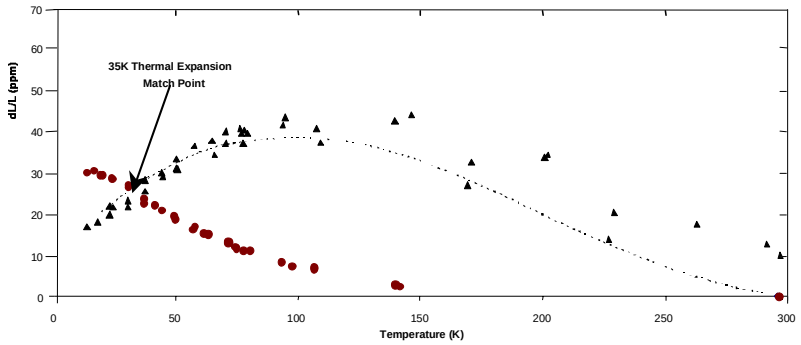

Figure 2-5 *Measured strain vs. temperature for a COI plated carbon fiber/cyanate ester laminate (triangles) tuned to match Zerodur (circles) at 35K. Dashed line traces the COI predictive model for the plated composite material.*

excessive strain introduced. Although graphite resins traditionally are subject to dimensional growth with moisture absorption, the current generation of graphite cyanate esters offers strategies to fully mitigate moisture absorption dimensional effects. We propose to use this combination of composite and Zerodur for CCM.

2.1.6 Mechanisms

The filter wheel assembly (FWA) is the one essential mechanism in CCM. Other mechanisms are discussed in the context of correction of system-level errors or uncertainties in optical alignment and pointing, but these are otherwise not required for the baseline science performance of CCM.

2.1.6.1 Cassini Heritage Filter Wheel

The FWA is capable of placing one of 16 selectable filter elements into the CCM optical beam at a pupil located 175 mm before the detector array focal plane. These elements include narrow and broadband optical filters, grisms, and special calibration optical elements designed to aid in the phase analysis of the NGST optical wavefront.

The spectral elements will include a set of broad (FWHM ~ 20% of the center wavelength) filters centered at 4.8, 4.2, 3.4, 2.1, and 1.6 μm respectively; spectral line filters for H Paschen-α 1.87 μm, H_2 2.12 μm, and [FeII] 1.64 μm; a number of grisms for R ~ 100; a blank (black) filter; and a number of optical elements to assist in high-order wavefront analysis and calibration. Furthermore, each filter is of sufficient diameter that a number of small calibration lamps can be positioned on the filter housing where they are visible to the detector through the periphery of the selected filter, yet they are clear of the optical beam from the telescope, to provide a uniform field calibration source for the detectors.

The CCM filter wheel assembly will be nearly identical to the filter assembly flown in the Wide Field Camera of the Cassini spacecraft, but modified for operation at cryogenic temperatures. It is functionally similar to the selectable optical filter assembly (SOFA) flown on the HST WF/PC and WFPC2 instruments. This design benefits from flight heritage at ambient temperatures and will utilize existing design practice and manufacturing processes developed for the flight qualification of similar mechanisms at cryogenic temperatures.

The unmodified Cassini filter wheel assembly consists of a stack of two independently controllable filter wheels. Each filter wheel is in effect a large diameter thin section three-phase stepper motor. The rotor web is machined to accept nine optical filter elements, each 43 mm diameter, that are clamped in place. Each rotor rotates independently, allowing any of the nine filter positions to be active in each wheel. One position in each wheel is open, providing sixteen positions for individually selectable filter elements. The selected filters are positioned in an off-center circular opening in the filter wheel housing.

For Cassini, the rotors were supported by wet-lubricated duplex pair ball bearings. A reflective-type redundant optical encoder provides position feedback. In this configuration, the LED light source and photodetector are mounted in a common housing located above the rotor. These housings are located near the outer diameters of the filter wheel housings and protrude axially. The rotor has a series of targets located adjacent to the filter openings, and by encoding a variety of patterns each filter is individually identified when it is in the open location. The filter wheel assembly

mounts into its mating structure through a series of flexures designed to isolate the assembly mechanically from any deformations and resulting loads including thermal deformations, vibration, and acceleration.

The vendor (Moog Schaeffer) will modify the Cassini filter wheel design to operate in NGST's 35 Kelvin environment. Mechanisms with elements common to the filter wheel assembly have been successfully developed and flown for cryogenic operations, including CLAES, COBE, and AIRS. The optical encoder is the only electronics mounted directly at the Cassini mechanism housing. This encoder, containing a feedback device requiring electronics, is unsuitable for environments below -55 degrees C. For CCM, the vendor will substitute an encoder design using optical fibers to remove the electronics from the cold environment entirely, relaying the optical signals to active devices in the warm electronics module. Adhesive bonding is not an acceptable attachment method at cryogenic temperatures due to differential thermal expansion between materials and expansion of the adhesive material, and because of other physical properties of the adhesives which change dramatically with temperature. All bonded joints will be replaced by clamped attachments, resulting in a slight increase in housing diameter and mass of the filter wheel assembly. Bearing mounting clearances require modification to provide proper fits at the reduced temperatures, and the wet lubricant will be replaced with a dry lubrication system such as MoS_2 or WS_2, a method that has been proven in the cryogenic applications mentioned above and also has been used in the HST/WFPC2 selectable filter wheel assembly. Estimated power consumption will be less than 100 milliWatts during active rotational stepping (100 Hz stepping rate to give 60° of rotation per second), and since filter rotations are done infrequently with a duty cycle of 0.01 or less, the power dissipation in the passively cooled ISIM enclosure will not be an issue. Finally, the filter clearances, alignments, and clamp attachments will be reviewed to account for any differential expansion. Though this indicates a substantial redesign of the Cassini unit, it is a design evolution that draws on existing flight hardware and specific heritage experience of the mechanism vendor.

2.1.6.2 WFPC2 Heritage Active Mirror

CCM provides the option to dither the image at the detector focal plane by incorporating a single mechanism to provide tip/tilt adjustment of fold mirror M3. This anticipated requirement comes from experience with infrared detector/multiplexer arrays, in order to provide for bad pixel (shorts, dropouts, etc.) replacement, small offsets (i.e. n + ½ pixels) to facilitate subpixel image sampling, and for a measure of freedom to select the best subarray on the detector chip. This feature has proven useful in the NICMOS camera. It is necessary to provide an internal dithering capability, since any dithering provided by the NGST will misregister CCM's occulting spot and the targeted object in the sky.

The fold mirror mechanism benefits from the design experience of the WFPC2 articulated fold mirrors (Fanson and Ealey 1993, Fanson and Trauger 1993). These mechanisms incorporated a mirror mount in the form of a monolithic invar flexure with three embedded PMN electroceramic actuators to provide $\pm 1 \times 10^{-3}$ radian range of mirror tilt. Stability and repeatability were on the order of 1×10^{-5} radians over periods of 2000 seconds. Three such AFMs have been in continuous service in HST/WFPC2 for over five years.

CCM requires a comparable range of tilt (a 1×10^{-3} radian tilt in M3 offsets the image by 22 pixels). CCM will require the replacement of the PMN electroceramic with a cryogenic material that is active at 35 Kelvins. Such cryoceramics are currently under development at Xinetics, Inc. as part of a technology thrust to meet the requirements for NEXUS and NGST deformable mirrors. Actuator elements with dimensions similar to the standard PMN elements, but fabricated with $SrTiO_3$ and KTaO, have been demonstrated as part of a NASA sponsored Small Business Innovative Research program, which is currently progressing from Phase 2 to Phase 3. This development program is expected to yield prototype actuator elements within the next year.

Power requirements are likely to be very low, since the actuator elements typically operate at low voltages (up to 30 volts) while exhibiting very low leakage (10^{10} ohms). Three precision voltage supplies mounted in the warm electronics bay will supply the necessary power. Power dissipation in the ISIM enclosure will be negligible.

The mechanism is multiply redundant, providing useful (but shorter range) actuation in the event of any single failed (shorted or open) actuator connection, and will provide a useful and stable mirror mounting with zero voltage inputs.

2.1.6.3 Lyot x/y Translation Stage

We assume that it will be necessary to carry out small on-orbit alignments of the CCM optical axis to the axis presented by the NGST/ISIM optics. Since the Lyot stop is most sensitive to alignment errors, a simple x/y translation mechanism is applied to the Lyot mask. Feedback on the centering of the Lyot mask on the NGST pupil image comes from analysis of calibration star images received by the science detector. This mechanism will be used only infrequently, and may be as simple as a pair of stepper motors driving lead screws through a flexure coupling. This mechanism poses no unusual challenges other than its operational temperature, and its use for infrequent calibration activities makes the power dissipation a minor issue. A generic part is costed for the baseline CCM, and there is no need to further define the mechanism at this time. Should the metrology of the ISIM be sufficiently well defined and known in advance, then it may be possible to eliminate this mechanism entirely from the CCM.

2.1.7 NIR Detector Characteristics

CCM covers the entire 0.8−5 μm spectral range with a single plate scale of 0.026″/pixel, selected for critical sampling at 2 μm wavelength. We find that the expected dark and read noise background in the detector array remains below the zodi background limit for the proposed HCOS science programs over the entire spectral range.

To first order, the detector performance specifications for CCM are similar to the direct imaging instruments for NGST. The spectral response should cover 0.8 to 5 microns, the quantum efficiency should be as high as possible with a target near 90%, the dark current must be less than the emission from zodiacal dust, placing an upper limit of order 0.03 electrons per second, and the read noise should be less than the shot noise associate with a few ×100 second integrations, yielding an upper limit of order 3 electrons.

Large format (2048^2 pixel) arrays which may meet NGST performance requirements are currently under development by various vendors. There are two competing technologies: mid-wave HdCdTe (doped for a 5.X micron cutoff) and InSb, which has a natural cutoff at 5.5 microns. Both technologies are under heavy development and both are likely to meet the first order requirements.

A modest model for the background entering the coronagraphic system indicates that the flux from the zodiacal background will range from a minimum of 0.03 electrons per second at 3 microns (in the “trough” between the scattered sunlight and thermal emission components of the zodiacal light) looking out along the zodiacal poles to 1.5 electrons per second at 5 microns through the zodiacal plane. This particular model assumes 0.026 arcsecond pixels with a filter passband of 20%. The zodiacal light properties are based on results from COBE, which to first order can be modeled as a 266 K graybody with an emissivity of 10^{-7} (thermal component) plus a 6200 K graybody with an “emissivity” of 3×10^{-14} (scattering component) along the plane, 1/3 of that value out of the plane. All other contributors, e.g. thermal emission from the telescope or other optical components, will be small in comparison.

The dark current requirements are quite strict given the above properties, particularly for the shorter wavelengths and narrow filters. Individual exposures are likely to be no more than a few hundred seconds, depending on the cosmic ray hit rate. Thus in the worst case, perhaps only 10 electrons will be collected in a few hundred second exposure in the dark areas of the sky. This provides an exceedingly difficult challenge to the detector multiplexer electronics as well as to the readout electronics and even the detector temperature stability (variations in the dark current rate will manifest themselves as an effective read noise). For CCM science targets, typical levels are a few tens to a few hundreds of electrons, in which case 3−5 electrons read noise would be acceptable (presumably through multiple sampling during the exposure, either Fowler sampling or sampling-up-the-ramp).

2.1.8 Image Stabilization and Pointing

By assumption, the NGST optical system provides a focal plane shared by all instruments in which all objects within a 4×10 arcminute field of view are stabilized to 0.0027 arcseconds rms.

Image stability at this specified level is a requirement for CCM performance, as it is for all ISIM instruments. In addition, CCM shares with the other instruments a requirement that lateral motion of the pupil be bounded to small excursions. In the CCM, pupil motion leads to a misregistration of the Lyot stop and the pupil image. In a spectrograph, pupil motion leads to undesirable variations in the illumination of gratings or other dispersive elements.

It has been recognized by the NGST project that the yardstick optical system, with a single fine steering mirror (FSM) for pointing correction, will not meet the ISIM pointing requirements. This is because (1) correction of body-pointing errors at a single field point by tip/tilt adjustment of a single FSM creates a correlated image tilt across the focal plane, and (2) geometric distortion across the field of view leads to differential errors in pointing correction across the field of view. Furthermore, pointing correction with a single FSM that is not located in a pupil plane creates correlated lateral displacements of the pupil images within each of the science instruments. Consideration of this design issue is beyond the scope of the ISIM studies, but we note that work in progress has identified practical alternative optical designs that appear capable of providing the required lateral stability in both the image and pupil locations over the entire NGST field of view. We have assumed that an alternate optical system such as this will be adopted by NGST. While our optical design uses and our concept graphics depict the yardstick optical system, our instrument design is valid for the (yet unspecified) alternative stabilization system as well.

2.1.9 Coronagraph Design

A coronagraph is defined by two essential elements—an occulting mask in the focal plane to reject the light from a bright central point source, and a Lyot stop at a subsequent pupil plane to remove the light that skirted the occulting mask due to diffraction by the telescope structures and mirror edges.

CCM uses a refined concept for the coronagraph, with an apodized or graded-density occulting mask at the first focus whose transmittance increases with radius, with the gaussian form $\tau = 1 - \exp[-(r /\sigma)^2]$. This simple refinement has profound effects on coronagraph performance. Because the mask is partially transmitting and smoothly graded, imaging continues to the center of the mask. This apodization concentrates the diffracted light more tightly near the edges of the pupil, where it is more effectively removed by the Lyot stop.

CCM requires an occulting spot with smooth optical density gradients that avoid granularity on physical scales as small as 1 μm. The optimal diameter for the occulting mask is wavelength dependent. CCM therefore includes occulting masks designed for best performance in the two primary science wavelengths of 2 μm and 4.5 μm. These are placed at two field positions separated by 10 arcseconds within the 52×52 arcsecond field of view. Telescope pointing will be used to select the appropriate occulting spot.

The Lyot mask is a simple element machined from a thin metal disk, to mask the edges of the primary mirror segments. The dimensions of the openings in the Lyot mask depend on the shape and optical characteristics of the telescope primary mirror and support structures. For this report, we have adopted a geometry that overlaps the outer 10% of the segment dimensions, resulting in an overall attenuation of approximately 50% of the incident light at the Lyot stop (see Fig. 2-6). A mechanism is provided to coalign the optical axes of NGST and CCM, so that the Lyot stop will be centered on the NGST pupil image.

2.1.10 NGST/CCM Imaging Simulations

Performance of the CCM coronagraph is fundamentally limited by speckle, the faint, noisy haze of light caused by coherent scatter from small irregularities on telescope optical surfaces. The NGST has baselined an active deformable mirror correction of its optical wavefront, and it will thereby suppress speckle to a maximum angular separation from the central star that corresponds to the density of actuators on the corrective mirror. It will clear a “dark hole” in the focal plane (Malbet, Yu, and Shao 1995). It is in this dark hole that CCM will provide its highest contrast imaging.

We seek a quantitative measure of the mirror surface irregularities that place meaningful limits on the science programs. The traditional measures of low-order surface errors, including rms surface roughness, Strehl ratio, sharpness ratio, and rms Zernike terms do not provide a useful metric for coronagraph performance. In fact, the coronagraph perfor-

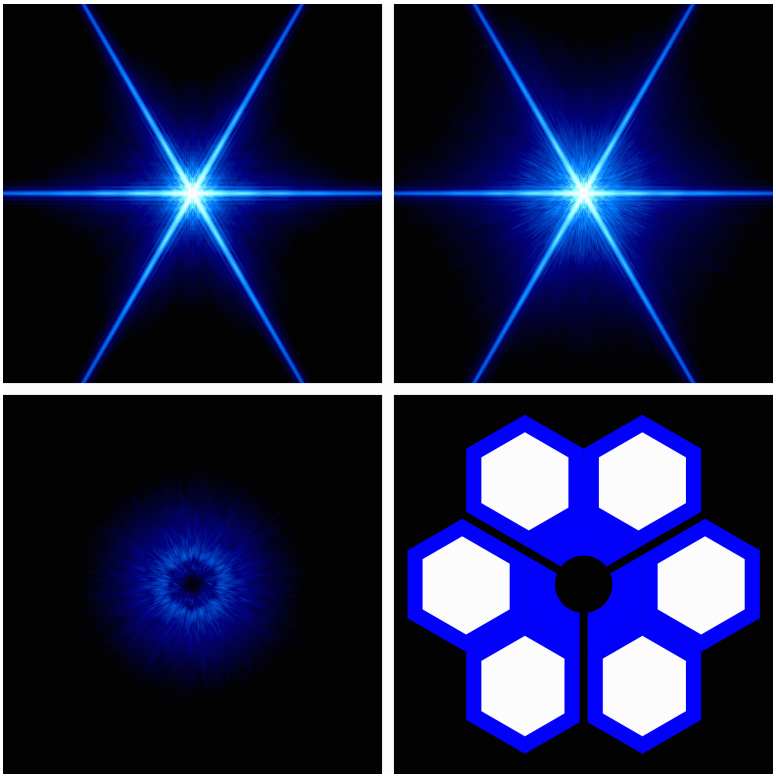

Figure 2-6 *Images of the NGST PSF (i.e. the image of a single star) at 2μm wavelength for three scenarios. Each of the three images shows the PSF over a 21.8″ square field of view. All intensities are shown with the same logarithmic contrast stretch. Upper left is the PSF for the NGST seven-segment design with perfect optical figure. Upper right is a more realistic estimate of the NGST PSF, including expected levels of mirror misalignments and surface polish and figure. The primary mirror follows the Arizona design concept, with 50 actuators per square meter to adjust the figure of a 2mm-thick glass facesheet, for which each actuator has a positioning resolution of 10 nm. The coronagraph field is seen at lower left. Here the bright central peak has been attenuated, revealing a coronagraphic "dark hole" created by the instrument optics and the deformable primary mirror. The diameter of the dark hole is proportional to the wavelength, hence the diameter in arcseconds of the dark hole would be 2.5 times larger at 5 μm wavelength. At lower right is the outline of the assumed NGST primary mirror, segmented into seven hexagons, each of which measures 3m edge-to-edge (TRW concept). Superimposed in blue is the coronagraphic Lyot stop, used internally in the coronagraph to reduce diffracted light from the telescope.*

mance is largely insensitive to small amounts of focus, jitter, astigmatism, etc. because these errors tend to rearrange the light in the core of the point spread function (PSF).

Instead, we note that in the smooth-surface limit, the angular distribution of the light scattered from the surface maps the power spectral density (PSD) of its residual surface roughness (Church et al 1979). We have obtained estimates of the PSD from a number of large-aperture high quality aspheric mirrors, such at the HST primary mirror (after the correction for its low order spherical error), and find that their PSD curves vs. spatial frequency often follow a power law at spatial frequencies greater than a few × 0.01 cycles/centimeter. We have adopted a "yardstick" surface figure metric by fitting a curve of the form of surface PSD = $A/[1+(k/k_0)^n]$ to the azimuthally averaged PSD from the HST phase map (e.g. Krist and Burrows 1995). We use this form to define an isotropic PSD approximation to the HST surface figure, with n = 3, $A = 5.8 \times 10^5$ A^2cm^2, and $k_0 = 0.03$ cycles/cm. We then use this metric to generate surface figure errors in our coronagraph simulation model. Figure 2-7 shows the HST-approximating curve (solid line). The data points have been taken from a mirror surface model generated with 10 times the surface PSD of HST and active surface figure correction with a deformable mirror (Arizona concept, 50 actuators/m^2, 10 nm actuator step size). The red curve, an azimuthal average of the data points, is the PSD estimate for the model mirror surface. The red curve drops below the 10 × HST PSD level at spatial frequencies less than a few × 0.01 cycles/cm. This is evidence of the effectiveness of the deformable mirror to reduce the surface scatter at low and mid spatial frequencies, and this dip in the PSD corresponds directly to the dark hole seen in an actively corrected telescope. The effect is seen in the simulated star images of Figure 2-6, and also in the corresponding

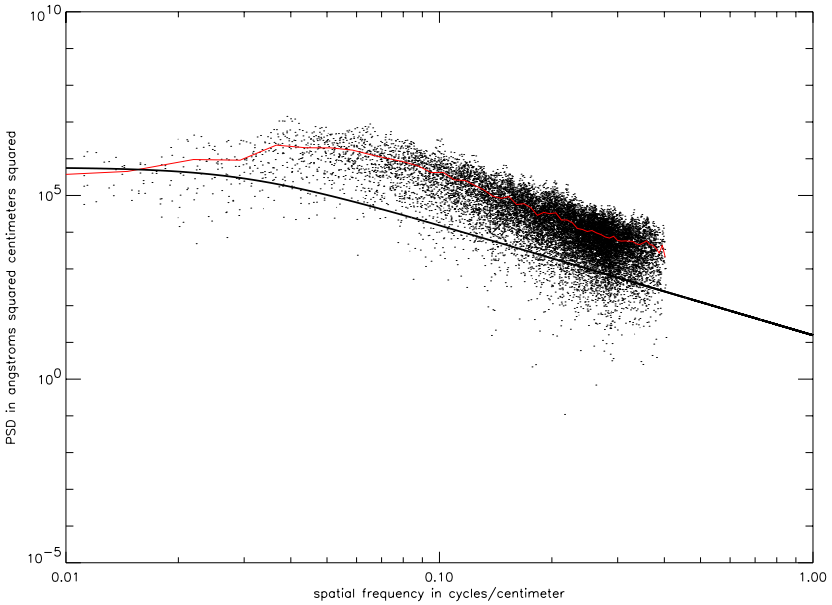

Figure 2-7 *Power spectral density of the NGST surface figure simulation. The red curve is the estimated PSD from the NGST simulations shown in Figures 2-6 and 2-8. For reference, the solid curve is representative of the HST mirror surface figure. At the higher spatial frequencies, the NGST model has 10× the PSD of the HST mirror, and at lower spatial frequencies, a PSD reduction is seen due to the active mirror correction.*

radial intensity plots for the coronagraph in Figure 2-7. NGST will use use a science imaging camera directly as a wavefront sensor, and the residual errors of this process must be included in the model imagery. A modified Gerchberg-Saxton (MGS) iteration is used, simultaneously operating on a pair of defocussed images (Gerchberg & Saxton 1972). The MGS algorithm will be used during by NGST (Redding *et al.* 1998). Use of defocussed imagery exposes structure in the beam that is normally lost in the glare of the central image spike, and allows separation of the multiple optical elements contributing to the overall wavefront error. This procedure avoids the need for dedicated wavefront sensing instrumentation, and provides a true end-to-end measure of the NGST/ISIM optical train.

Given this statistical representation of mid-spatial-frequency surface figure, and having accounted for the NGST mirror alignment process, our NGST/CCM model then simulates NGST imagery by including effects of detector pixel sampling, coronagraph occulting and Lyot masks, optical aberrations and tolerances, measured and generated mirror surface errors, pointing jitter, detector characteristics including read noise and dark background rates, and photon statistics and spectral character of the calibration reference stars. The optical surface deformations of the deformable mirror have been characterized in terms of a structural finite-element model constrained by laboratory measurements. It is this model that has been used estimate the science performance of the NGST and the CCM.

2.2 Technology Readiness

The CCM as described here can be developed without the invention of significant new technologies. Some of the optical elements have challenging figures to manufacture, the dither mirror M3 depends on the successful demonstration of cryo-electroceramic actuators, the expected NIR detector array performance is central to the science of CCM.

However, the CCM science performance depends most directly on the quality and stability of the baseline wavefront correction, hence CCM is dependent on the state of the art for deformable mirrors, either in the form of a primary mirror with an active facesheet, or in the form of a small deformable mirror mounted within the ISIM optical path. As CCM is described here, active wavefront correction is provided exclusively by the NGST system, hence it is formally beyond the scope of an ISIM concept study. The science program simulations that appear in Section 1 indicate that science performance is strongly dependent on three primary wavefront metrics. The primary mirror surface figure is the main source of scattered light within the first few arcseconds of a star. The surface figure of the primary was generated with a PSD approximately equal to that of the HST primary and other recent large astronomical mirrors for the EGP/BD survey in Section 1.2.1, and approximately 10 times worse in all the other simula-

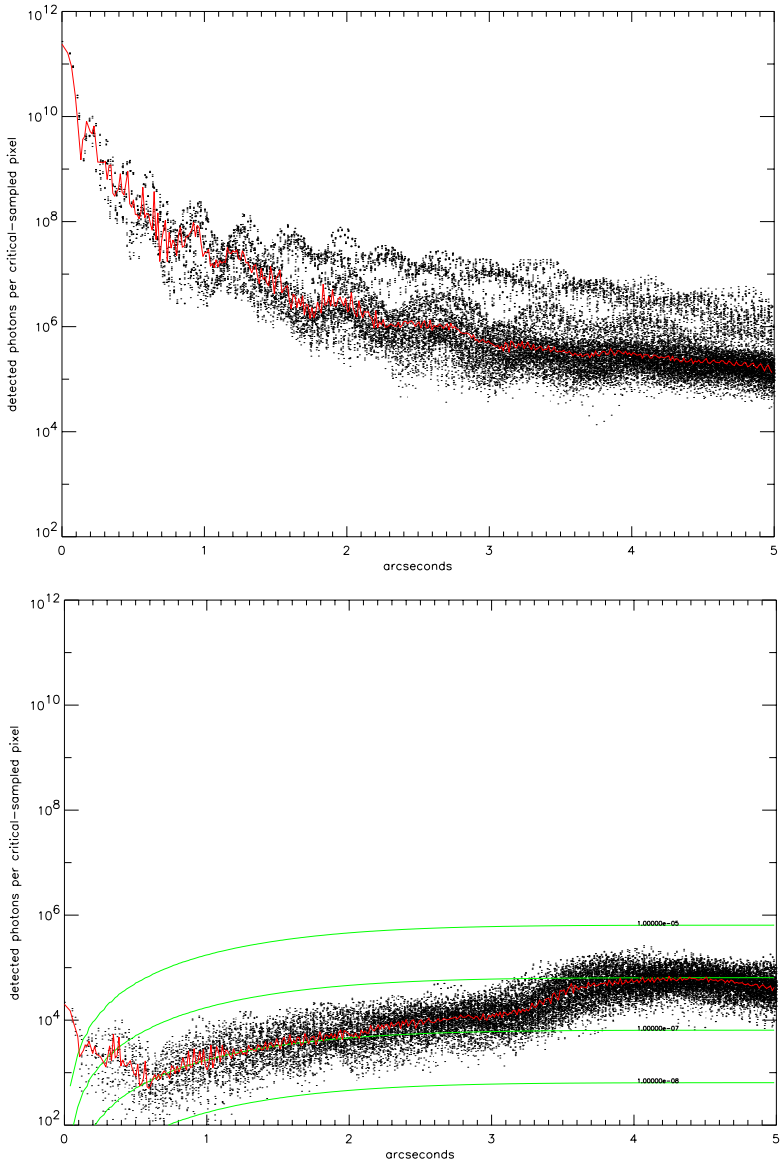

Figure 2-8 *Predicted point spread function (PSF) intensity vs. radius for NGST and with and without the coronagraphic correction. Upper panel shows the nominal NGST PSF at 4.95μm wavelength, following the on-orbit alignment of the mirror segments. The lower panel is the same as above, but with the addition of the coronagraph optics. Median intensities as a function of radius are traced by the red curves, while the green traces indicates the intensity vs separation for a companion to the central star that is fainter than the star by the indicated factors.*

tions. Second, the area of the "dark hole" cleared by deformable mirror adjustments is roughly proportional to the number of actuators distributed across the telescope pupil, with ~ 2000 actuators in play in our science simulations. Third, the depth of the high-contrast dark hole is roughly follows the square of the actuator positional errors, or equivalently the magnitude of the PSD at the spatial frequencies within the dark hole. Our simulations assumed an actuator step size of 10 nm for all simulations except the EGP/BD survey, where they were an order of magnitude smaller.

Deformable mirrors with ~ 1000 actuators capable of positional accuracies of several Angstroms rms in a stable space environment are readily available from Xinetics, Inc. and widely in use at groundbased observatories. Ongoing development of electroceramic materials that are active at NGST's 35K operating temperature are very promising, with $SrTiO_3$-doped articles already in test. Other proprietary technologies are undoubtedly in development as well. The development of a stable, accurate, high-density deformable mirror technology is crucial to the success of NGST and large-aperture space observatories in general. NASA's thrust to develop deformable mirrors for NGST is of critical importance, if a stable high-density deformable mirror technology is to be available when it is needed by NGST in the next 2–3 years.

2.3 Development Schedule and I&T Plan

The CCM development flow will be assured by early planning and scheduling, as well as early consideration of the developing ICDs and GSE resources that will be shared among the instruments. Camera and coronagraph will be developed as subassemblies, then integrated into the CCM system truss.

In Phase A, the System level considerations will define the ISIM placement and final configuration of the instrument truss, attachment points, power access, the allocated volume in the warm electronics bay as required for the CCM system, including the detector and mechanism drives. CCM system requirements will be reviewed in light of the selected NGST observatory architecture. A calibration strategy will be devised that assures that components, subassemblies, and system level functionality are characterized at the most efficient points in their development, with the goal of the ultimate delivery of a calibratable and fully calibrated instrument. Early scheduling of use of any shared GSE test resources and integration into the CCM development schedule will help avoid problems as delivery deadline approach. A strong engineering staff will be identified in preparation for final Phase A and Phase C scheduled activities. Meanwhile, for the camera subsystem, Phase A work begins with a detailed optical design and optimization, including consideration of any challenging mirror manufacturing, mounting, and alignment requirements. The three mirror anastigmat optical subassembly will be designed. Tip/tilt mirror development will begin with the identification, procurement, and test of the actuator electroceramics, followed by a flexure design that is tuned to the optical requirements and actuator capabilities. A detailed specification of the optical filter set will be created, and the filter wheel mechanism vendor will be authorized to design and test the engineering modifications for cryogenic operation. NGST/ISIM interface control documents (ICDs) will be collected and optical, electrical, and mechanical system interfaces will be designed. A test plan will be devised that makes optimal the use of GSE metrology fixturing and GSE test and verification services, and a verification matrix will be devised to assure that all CCM system specifications are validated by test or analysis as appropriate.

The coronagraph Phase A activity, as for the camera, will begin with the optical and mechanical design of the pickoff and toroid mirrors, and a detailed analysis and plan for stray and scattered light control in the foreoptics light path. ICD negotiations will be carried out to ensure that the pickoff mirror assembly is compatible with the requirements of all instruments for access to the focal plane. The occulting mask will be specified and procured during Phase A, allowing a maximum period for the refinement of the optical performance of this small part. The design and vendor for the Lyot mechanism will be selected. The optical, electrical, and mechanical system interfaces will be designed with reference to the ICDs.

Following the CDR, during Phase C all parts and subsystems will be procured, and the development and testing will flow according to the Phase A planning. Flight qualification of mechanisms, electronics, structural components, optical mountings, will be carried out. Optical performance will be verified at the component and subsystem levels. Control sequences and software will be developed. Camera and coronagraph subassemblies will be integrated into the system truss. Optical and mechanical alignment will be tested against GSE metrology fixtures. An instrument system-level cryogenic vacuum test facility will be reserved and modified as required for 35K operation. System-level tests and calibrations will be carried out, results compiled for review and delivery to GSFC, and science calibration data analyzed and distributed to the STScI. Advance planning, early scheduling of long lead items, and close coordination with the NGST project will produce and deliver an instrument ready to deliver pioneering discoveries with NGST.

3. COST ESTIMATE

3.1 Cost Summary

A ROM cost for CCM has been figured with the following assumptions. A single flight unit will be produced, with brassboard and proof of concept prototypes as required. A NIR detector array, control and signal electronics, and data system are provided GSE. CCM will engineer the detector enclosure, using GSE thermal control. Mechanism electronics will be fabricated and flight qualified by CCM, while the conditioned power and control processor is suppplied as GSE. CCM will be designed for compatability with the NGST/ISIM ICD, and all structures and assemblies will be fabricated and tested to instrument system level by CCM. The CCM manufacturing philosophy is based on a mechanical structure that is assembled and optically aligned in an ambient laboratory environment, flight qualified at room tmperature, then validated for cryogenic operation in a dedicated thermal vacuum test. It is assumed that a metrology reference fixture will be supplied GSE as a guide for optical and mechanical interface metrology. The years 2001–2003 are devoted to subsystem design and prototype development, including the detector enclosure, mechanisms, power supplies, and optical design, leading up to CDR. The CCM will be fabricated and tested during the years 2003–2005, leading to delivery of a flight qualified and science calibrated instrument to GSFC in June 2005. Science team will provide oversight throughout the program, ramping up to GTO planning activity in the final 18 months prior to a December 2007 launch. We have separated the program into four main cartegories: System level engineering/management and integration, camera subsystem manufacture, coronagraph subsystem manufacture, and science oversight/planning. We specify a 20% reserve. All labor is fully burdened. Figures are quoted in FY99 $K. Bottom line numbers, drawn from the more detailed cost breakdown in section 3.2, are as follows:

1.0 CCM System	$10,854
2.0 Coronagraph subsystem	2,799
3.0 Camera subsystem	7,810
4.0 Science	2,196
TOTAL	23,659
5.0 Reserve (20%)	4,732
TOTAL + RESERVE	$28,391

3.2 WBS and Cost Breakdown

HCOS CORONAGRAPH INSTRUMENT WBS	Senior Engineer FTE (yrs)	Technical/ Adminis-trative FTE (yrs)	Non-Labor Costs	Subtotals	Totals
1. SYSTEM LEVEL					$10,854.4
1.1. Project management	4	1	150.0	1,082.0	
1.2. System engineering	4	1	150.0	1,082.0	
1.3. Risk management and reliability	0.2	0	10.0	50.8	
1.4. Product assurance	0.8	1	50.0	334.0	
1.4.1. Contamination control plan	0.2	0.3	50.0	130.0	
1.4.2. Safety	0.1	0.1	5.0	37.4	
1.5. Documentation	0.5	1	50.0	274.0	
1.6. Telescope ICD and envelope drawing	0.2	0.4	5.0	93.4	
1.7. Signal interface box (warm) GFE	0.25	0	0.0	50.0	
1.8. Structures					
1.8.1. Interface to ISIM	0.2	0.3	10.0	86.8	
1.8.2. Optical enclosure	0.4	0.4	275.0	425.0	
1.8.3. Truss structure	0.4	0.25	900.0	1,082.0	
1.9. Optical/stray light design	0.4	0.4	85.0	219.8	
1.10. Systems level mechanical design	1	2.5	40.0	543.2	
1.11. Thermal design	0.2	0.2	0.0	64.0	
1.12. Contamination control	0.15	0.2	50.0	108.0	
1.13. Integration and test	2.2	4	1,200.0	2,216.0	
1.13.1. Test fixtures (for GSE stimulus)	0.5	0.5	100.0	268.0	
1.14. Environmental test	1	1.5	300.0	704.0	
1.14.1. LHe, LN2, supplies	0.02	0.05	250.0	280.0	
1.15. Post delivery support	0.5	1.5	100.0	388.0	
1.16. Brass boards and proofs of concept	0.5	1	500.0	760.0	
1.17. Calibration, on-orbit verification	1.5	0.5	200.0	576.0	
2. CORONAGRAPH SUBSYSTEM					$2,799.0
2.1. Package/baffling/light shroud	0.35	0.4	72.0	195.8	
2.1.1. Structures and housing	0.2	0.1	300.0	376.0	
2.2. Pick-off mirror					
2.2.1. M1 mirror assembly	0.2	0.3	64.0	145.1	
2.2.2. Special baffling for foreoptics	0.2	0	220.0	277.6	
2.3. Occulting spot assembly	0.5	0.6	80.0	258.4	
2.4. M2 assembly	0.15	0.3	96.0	169.7	
2.4.1. Toroid mirror M2	0.15	0.3	275.0	363.0	
2.5. Lyot stop					
2.5.1. Stop assembly	0.2	0.4	85.0	179.8	
2.5.2. Lyot x/y drive					
2.5.2.1. Drive	0.2	0.4	120.0	217.6	
2.5.2.2. Drive electronics	0.35	0.4	150.0	280.0	
2.6. Subsystem qualification testing	0.3	0.5	200.0	336.0	

HCOS CORONAGRAPH INSTRUMENT WBS	Senior Engineer FTE (yrs)	Technical/ Adminis-trative FTE (yrs)	Non-Labor Costs	Subtotals	Totals
3. F/18 CAMERA SUBSYSTEM					$7,810.7
3.1. Package/baffling/light shroud	0.25	0.3	65.0	156.2	
3.1.1. F/18 camera subassembly and housing	0.5	0.5	300.0	484.0	
3.2. Fold mirror					
3.3. M3 assembly	0.4	0.65	305.0	487.4	
3.3.1. M3 tip/tilt drive	0.5	1	400.0	652.0	
3.3.2. Tip/tilt electronics	0.4	1.5	500.0	800.0	
3.4. F/18 Three Mirror Anastigmat (TMA) camera					
3.4.1. TMA assembly	0.5	0.5	225.0	403.0	
3.4.2. Mirror A1	0.33	0.15	450.0	570.0	
3.4.3. Mirror A2	0.33	0.15	600.0	732.0	
3.4.4. Mirror A3	0.33	0.15	800.0	948.0	
3.4.5. Optical test design	0.4	0.05	100.0	194.0	
3.5. Filter wheel assembly					
3.5.1. Mechanism	0.2	0.25	300.0	394.0	
3.5.2. Filter set (16 filters)	0.2	0.4	240.0	347.2	
3.5.3. Drive electronics (warm box)	0.65	0.6	187.0	404.0	
3.5.5. Assembly	0.1	0.1	24.0	57.9	
3.6. Focal plane enclosure	0.2	0.15	32.0	92.6	
3.6.1. Detector housing	0.2	0.15	75.0	139.0	
3.6.2. Thermal strap	0.1	0.1	3.0	35.2	
3.6.3. Signal/power cables	0.1	0.1	15.0	48.2	
3.7. Assembly	0.6	1	250.0	510.0	
3.8. Subsystem qualification testing	0.4	0.5	200.0	356.0	
4. SCIENCE					$2,196.0
4.1. Calibration	1.5	4	200	996.0	
4.2. Science program	1.5	5	300	1,200.0	
				TOTAL	$23,660.1
4. RESERVE (20%)				$4,732.0	
				TOTAL + RESERVE	$28,392.1

4. REFERENCES

Alcolea, J. & V. Bujarrabal, 1991, A &A 251, 536

Allard, F., P.H. Hauschild, I. Baraffe, & G. Chabrier, 1996, ApJ (Letters), 465, L123

Angel, J.R. and J. Burge, 1999, "Ultraviolet-Optical Space Astronomy Beyond HST," ASP Conference Series 164, ed. J. Michael Shull, Anne L. Kinney, & Jon A. Morse, p. 234

Angel, J.R. and N.J. Woolf 1997, ApJ, 475, 393

Angel, J.R.P. 1994, Nature 368, 203

Backman, D.E. 1998, in "Exozodiacal Dust Workshop Conference Proceedings," eds. D.E. Backman et al., *NASA/CP-1998-10155, pp. 107–120*

Backman, D.E., and F. Paresce, 1993, in "Protostars and Planets III," E.H. Levy and J.I. Lunine eds, University of Arizona Press, Tucson, pp. 1253–1304

Bahcall, J., S. Kirhakos, D. Saxe, and D. Schneider, 1997, ApJ, 479, 642

Bahcall, J.N., et al., *ApJ, 387, 56*

Bahcall, J.N., et al. *1997, ApJ Letters 386, L1*

Bartelmann, M. and A. Loeb, 1998, ApJ, 503, 48

Baugh, C., S. Cole, C. Frenk, and C. Lacey, 1998, ApJ, 498, 504

Beckwith, S., A.I. Sargent, R. Chini, and R. Gusten, 1990, AJ, 99, 924

Beichman, C.A. (ed.) 1996, A Road Map for the Exploration of Neighboring Planetary Systems (ExNPS), JPL Publication 96-22

Beichman, C.A., N.J. Woolf, and C.A. Lindensmith (eds) 1999, "The Terrestrial Planet Finder (TPF)" JPL Publication 99-3

Brown, R.A. & C.J. Burrows, 1990, Icarus, 87, 484

Burgasser, A.J., et al. *1999, ApJ, 522, L65*

Burrows, A., M. Marley, W.B. Hubbard, J.I. Lunine, T. Guillot, D. Saumon, R. Freedman, D. Sudarsky, C. Sharp, 1997, ApJ, 491, 856

Burrows, A., W.B. Hubbard, D. Saumon, & J.I. Lunine, 1993, ApJ, 406, 158

Burrows, C.J. et al. *1995, BAAS 187 3205*

Burrows, C.J. et al. *1996, ApJ, 473, 437*

Butler, R.P., G.W. Marcy, D.A. Fischer, T.W. Brown, A.R. Contos, S.G. Korzennik, P. Nisenson, R.W. Noyes, 1999, submitted to ApJ

Chan, S.J., & S. Kwok, 1988, ApJ, 334, 362

Church, E.L., H.A. Jenkinson, and J.M. Zavada, 1979, Opt Eng, 18, 125

Cochran, W.D., A.P. Hatzes, R.P. Butler, G. Marcy, 1997, ApJ, 483, 457

Dermott, S.F. et al. *1998 in "Exozodiacal Dust Workshop Conference Proceedings," eds. D.E. Backman* et al., *NASA/CP-1998-10155, pp. 59–84*

Dodson, K., G. Mehle, and E. Kasl, 1999, Proceedings of the SPIE meeting, Denver

Dominik, C. 1998, poster presentation at Protostars and Planets IV

Efstathiou, G. and M.J. Rees, 1988, MNRAS, 230, P5

Fanson, J. and M. Ealey, 1993, Proceedings of the SPIE, Vol. 1920, Albuquerque

Fanson, J. and J. Trauger, 1993, Proceedings of the SPIE, Vol. 1996, San Diego.

Gerchberg, R.W., and W.O. Saxton, 1972, Optik 35, 237–246

Gliese, W., and H. Jahreiss, 1979, Astron. Astrophys. Suppl. 38, 423

Greaves, J.S. et al. *1998, submitted to ApJ Letters*

Greenhouse, M. et al. *1998, Proceedings of the 34th Liege Colloquium (ESA SP-429), 275*

Haehnelt, M.G., and M. Rees, 1993, MNRAS, 263, 168

Hartwick, F.D.A., and D. Schade, 1990, ARAA 28, 437

Holland, W.S. et al. *1998, Nature 392 788–790*

Hora, J. et al. *1999, in "Asymmetrical Planetary Nebulae II: From Origins to Microstructures," MIT, Cambridge, MA, USA, Aug 3–6, 1999*

Hrivnak, B.J., S. Kwok, K.M. Volk, 1989, ApJ, 346, 265

Jura, M. 1986, ApJ, 309, 732

Jura, M. & S.G. Kleinmann, 1989, ApJ, 341, 359

Kaiser, N., 1984, ApJ Letters, 284, L9

Krist, J., and C.J. Burrows, 1995, Applied Optics, 34, 4951

Krist, J.E., D.A. Golimowski, D.J. Schroeder, and T.J. Henry, 1998, PASP (in press)

LeBoeuf, C., P.S. Davila, D.C. Redding, D.R. Coulter, L. Pacini, 1998, SPIE paper 3356-72, Kona HI

Lopez, B., W.C. Danchi, M. Bester, et al. *1997, ApJ, 488, 807*

Malbet, F., J. Yu, and M. Shao, 1995, PASP 109, 386

Marcy, G., and P. Butler, 1998, Ann. Rev. Astron. Astrophys. 36, 56

Marley, M.S., G. Christopher, D. Stephens, J.I. Lunine, and R. Feedman, 1999, ApJ, 513, 879

Marley, M.S., D. Saumon, T. Guillot, R.S. Freedman, W.B. Hubbard, A. Burrows, J.I. Lunine, 1996, Science, 272, 1919

Mayor, M. and D. Queloz, 1995, Nature, 378, 355

McCaughrean, M.J., K.R. Stapelfeldt, and L. Close, 1999 in Protostars and Planets IV, V. Mannings, A. Boss, and S. Russell eds., Univ. of Arizona Press, Tucson, in press

McCaughrean, M.J. & C.R. O'Dell, 1996, AJ, 111, 1977

Mosier, G.E., M. Femiano, K. Ha, P.-Y. Bely, R. Burg, D.C. Redding, A. Kissil, J. Rakoczy, L. Craig, 1998, SPIE paper 3356-08, Kona HI

Moutou, C., A. Boccaletti, and A. Labeyrie, 1998, Proceedings of the 34th Liege Colloquium (ESA SP-429), 211

Nakajima, T., B.R. Oppenheimer, S.R. Kulkarni, D.A. Golimowski, K. Matthews, S.T. Durrance, 1995, Nature, 378, 463

Oppenheimer, B., S.R. Kulkarni, K. Matthews, M.H. van Kerkwijk, 1998, ApJ, 502, 932

Ortiz, J.L., G.S. Orton, A.J. Friedson, S.T. Stewart, B.M. Fisher, J.R. Spencer, 1998, JGR, 103, No. E10, 23051

Paresce, F. 1990, ApJ, 357, 231

Paresce, F. & W. Hack, 1994, A &A, 287, 154

Rabbia, Y., P. Baudoz, and J. Gay, 1998, Proceedings of the 34th Liege Colloquium (ESA SP-429), 279

Ray, T.P., R. Mundt, J.E. Dyson, S.A. Falle, and A.C. Raga, 1996, ApJ, 468, L103

Reach, W.T. 1998 in "Exozodiacal Dust Workshop Conference Proceedings," eds. D.E. Backman et al., *NASA/CP-1998-10155, pp. 25–43*

Redding, D., S. Basinger, A. Lowman, A. Kissil, P. Bely, R. Burg, G. Mosier, M. Femiano, M. Wilson, D. Jacobson, J. Rakoczy, J. Hadaway, 1998, SPIE paper, 3356–47, Kona HI

Roddier, F., C. Roddier, M.J. Northcott, J.E. Graves, and K. Jim, 1996, ApJ, 463, 326

Sahai, R., J.T. Trauger, A.M. Watson, et al. *1998a, ApJ, 493, 301*

Schneider, G., B.A. Smith, E.E. Becklin, D.W. Koerner, R. Meier, D.C. Hines, P.J. Lowrance, R.J. Terrile, R.I. Thompson, M. Rieke, 1999, ApJ, 513, L127

Seery, B.D. 1998, SPIE paper 3356-01, Kona HI

Shu, F.H., H. Shang, T. Lee, 1996, Science, 271, 1545

Soker, N. 1996, ApJ, 460, L53

Soker, N. & M. Livio, 1994, ApJ, 421, 219

Stapelfeldt, K.R. et al. *1998, ApJ, 502, L65*

Stockman, H.S. (ed.) 1997, The Next Generation Space Telescope, STScI

Strauss, M.A. et al. *1999, ApJ, 522, L61*

Strom, K.M., S.E. Strom, S. Edwards, S. Cabrit, and M. Skrutskie, 1989, AJ, 97, 1451

Trauger, J., R. Sahai, K. Stapelfeldt, D. Moody, and J. Lunine, 1999, Design Reference Mission Proposal for NGST

Tsuji, T., K. Ohnaha, W. Aoki, & T. Nakajima, 1996, A&A, 38, L29

Welch, C., A. Frank, J.L. Pipher, W.J. Forrest, and C.E. Woodward, 1999, ApJ, 522, L69

Werner, M.W. 1998 in "Exozodiacal Dust Workshop Conference Proceedings," eds. D.E. Backman et al., NASA/CP-1998-10155, pp. 219–232

Woolf, N.J. and J.R. Angel, 1998, Ann.Rev.Astron.Astrophys. 36, 507